National Institute for Occupational Safety & Health
Contract Number: 5 R01 OH07787
Grant Number: GRT960769
Research Foundation Project Number: 743883
09/30/2002 – 09/29/2007

Final Report

Derived Spine Loads in Response to Multiple Risk Factors

William S. Marras, Ph.D.
Biodynamics Laboratory
The Ohio State University
1971 Neil Avenue
Columbus OH 43210
614-292-6670
marras.1@osu.edu

Waldemar Karwowski, Ph.D., and Jacek M. Zurada, Ph.D.
University of Louisville

Kermit G. Davis, Ph.D.
Low Back Biomechanics and Workplace Stress Laboratory, University of Cincinnati

January 2008

Table of Contents

Abstract

Low back disorders are extensive and extremely expensive for industry. As such, there is a need for better techniques that can assess structural loading in the industrial setting. To date, investigation of the loading on the back has been with simple static models that neglected the complex coactivity patterns of the trunk musculature. Thus, the objective of the current project was to develop a neuron-fuzzy engine that could predict the muscle activation pattern for common lifting conditions. The predicted muscle activation data can then be input into the EMG-assisted model to predict the spine loads.

The **first specific aim** was to develop an artificial neural network model in the form of a multi-stage hybrid neuro-fuzzy "engine"—HNFE for electromyography (EMG) signal estimation was built using kinematic, kinetic, anthropometric, and work condition variables as inputs including physical and psychosocial characteristics. A complex engine was developed using fuzzy average with fuzzy cluster distribution techniques in combination with neural network structure. In order to identify inputs that have significant influence on the output, a method using fuzzy average with fuzzy cluster distribution (FAFCD) was utilized. The FAFCD method allows for the reduction of a high dimensional input space so that more effective models for EMG estimation can be built. After key work condition variables affecting EMG in lifting tasks were found using this method, a novel structure of feed forward neural network was utilized to estimate the instantaneous EMG by evaluating the full lifting motion at one time rather than estimating one sampling point at a time. The complete neural network model accounts for both global and local features of the input data. The resulting neural network model has the capability of predicting muscle activity from the input variables: kinematic, kinetic, and anthropometric factors under a wide variety of lifting conditions. For all muscles, the overall average MAE is 7.56%; the overall average R-square is 0.5437. Thus, the model was designed to be accurately and robust with respect to predicting the muscle activity values under realistic lifting conditions.

The **second specific aim** was to establish the large database that was utilized to develop the multi-stage hybrid neuro-fuzzy "engine". The entire data set is both extensive and robust with respect to the parameter space. While not all work conditions imaginable were incorporated into the training sets utilized to develop the HNFE, the boundaries of the data set encompasses the majority of lifting conditions found in the workplace. The conditions that were utilized to train the model serve as the boundary conditions. The model can then interpolate between the conditions to predict muscle activity of new conditions, reducing the necessity to collect an all encompassing data set. The structure of the model also allows the model to be continually trained when new data is acquired.

The **third specific aim** was to develop software that will link the HFNE to a website to allow for users to predict the muscle activities based on their data that could be utilized for the prediction of spine loads with their own spine load model or with the OSU EMG-assisted spine load model. A software program has been linked to a website where users can predict muscle activity from the ten trunk muscles during specific work conditions as well as upload new data to train the fuzzy engine.

The **fourth specific aim** was to link the HFNE to the OSU EMG-assisted model and compared the loads predicted from the original EMG values to the predicted HFNE EMG

values. The model fidelity was actually improved with the predicted EMG as compared to the actual EMG with improved r-square and average absolute error values. Furthermore, the three-dimensional spine loads were almost identical for the predicted EMG as compared to the actual EMG (within 35 N in each plane). The compression forces predicted within 1% while shear forces were within 11%.

In all, the project develop a very robust model that can now predict muscle activity for lifting conditions in industry where previous techniques were significantly limited to lack of technology, need for expensive equipment, and interference from surrounding machinery. Thus, by integrating the HNFE into a state-of-the-art spine loading model, it will now be possible to accurately estimate the loads on the spine in real world lifting conditions.

Significant Findings

The project has developed a sophisticate "engine" that predicts the complex muscle activation pattern for the most common lifting conditions found in industry. The new hybrid neuro-fuzzy "engine" (HFNE) has the capability to predict muscle activities of the ten trunk muscles based on continuous kinematic (position and motion of the trunk) and kinetic (external loads on the back) data, workplace conditions (e.g. task asymmetry, weight lifted, lifting technique, stress level, mental demands, etc.), and subject anthropometry (e.g. stature, weight, etc.). The HFNE accurately predicted the muscle activity for a robust data set that will ensure the accurate prediction of muscle activities during lifting in industry. The HFNE has been linked to a website so that users can upload data and acquire predictions of the trunk muscle activities. Further, the predicted muscle activity was accurately predicted and produced almost identical spine loads as the actual (collected) data when input into the EMG-assisted model.

Translation of Findings

For the first time, the neuro-fuzzy network engine provides the capability for researchers to know account for the muscle coactivation patterns that accompany dynamic and complex lifting. The HFNE predicts the muscle activity level of the ten major trunk muscles under conditions where employment of electromyographic techniques would be virtually impossible. The method requires only some basic body dimensions, descriptions of the workplace conditions, measurement of the three-dimensional trunk motions and trunk moments through well-established and quantitative techniques. Quantification of muscle activity in dynamic, industry settings will finally allow accurate estimates of spine loads that the workers are exposed to and therefore can be utilized to quantify risk of low back injuries better.

Outcomes and Relevance

The project developed a neuro-fuzzy network engine that accurately predicts the muscle activity of the ten trunk muscles. The HFNE provides the first tool to accurately estimate muscle activity in industry without the worry of artifacts and other factors that significantly plague traditional EMG acquisition.

Background

Back injuries are common in industry and extremely costly. Back pain has been described as one of the most common and significant musculoskeletal problems in the United States leading to substantial amounts of morbidity, disability and economic loss [1, 2]. Back disorders were responsible for the loss of half a billion lost workdays in 1988 with 22 million cases reported that year [3]. Among people under 45 years of age, LBD is the leading cause of activity limitation and effects up to 47% of workers with physically demanding jobs [4]. Pope [5] has reported that the prevalence of LBD has increased by 2700% since 1980. The costs associated with LBD are enormous. Early estimates of lost wages alone, amount to four billion dollars annually [6]. Webster and Snook [7] estimated that in 1986 the average direct costs of LBD was $6,800 per case. Recent estimates of societal costs range from 25 to 95 billion dollars per year [8].

Risk factors in the workplace

The risk of LBD is associated with industrial work [4]. Thirty percent of occupational injuries in the United States are caused by overexertion, lifting, throwing, holding, carrying, pushing, and or pulling objects that weigh 50 pounds or less [9]. Low back disorders are associated with occupational materials handling. The epidemiologic literature [10-12] has noted that the type of work involved in an occupation is closely associated with the risk of suffering a LBD. In particular, manual materials handling (MMH) activities dominate occupationally related LBD risk. It is estimated that lifting and MMH account for 50% to 75% of all back injuries [13-15].

Specific physical workplace characteristics have been associated with LBD risk [16-19]. A series of industrial surveillance studies have been able to describe the physical workplace parameters (lift origin height, lift destination height, lift frequency, lift asymmetry, weight of object lifted, load moment, etc.) and their association with risk [16-19]. In addition, these same studies have been able to document the association between trunk kinematics and LBD risk. A multiple logistic regression model has been developed based upon these studies that have been able to describe how risk changes as the combination of these workplace features and trunk kinematic characteristics change [16-18]. Similar findings were reported by Norman and associates in an independent study [19]. These studies have shown that the better one described the physical job demands, the better the association with risk of LBD. These risk models have documented the levels at which each five variables (lift rate, trunk twisting velocity, trunk lateral velocity, load moment, and sagittal flexion angle) become problematic.

Laboratory studies have been able to explain how these physical workplace characteristics can increase the risk of LBD. Biomechanical studies have been able to show how the trunk muscle recruitment patterns and coactivations as well as the subsequent spine loadings can impose loads on the spine [20-25] that would be expected to exceed the vertebral end plate tolerance limits when exposed to the risky levels of these five risk variables identified in industrial surveillance studies [16-18, 26]. In addition, a number of laboratory studies have been able to document how trunk muscle recruitment and high levels

of trunk muscle coactivation can result in excessive spine compression and shear forces under various materials handling situations. These situations include materials handling of cases [27-31], team lifting [32], patient lifting [33], and lifting under various kinematic conditions [34-36]. Under all of these conditions, increased in spine loading was a result of increased muscle coactivation during the materials handling activity.

Psychosocial linkages to back pain have also been established [13, 37-47]. Recent prospective studies have shown that both biomechanical factors and psychosocial factors can independently predict LBD [68]. However, most researchers feel that biomechanical risk factors must be present before psychosocial factors are able to play a role. Thus, biomechanical loading is believed to be the primary injury pathway for occupationally related LBDs. This logic has been reinforced through laboratory studies that have monitored the muscle activities and subsequent spinal loadings associated with psychophysically based decisions [31, 48-50]. These studies have shown that psychophysical decisions are associated with muscle responses yet not necessarily spinal loading. Hence, these studies show that subject perception does influence muscle activity but perception alone cannot reflect trunk loading and risk of injury very well. Recent studies have also shown that psychosocial factors such as interpersonal communication (social context) [42] and mental stress due to pacing and precision of work (organizational factors) [51] can influence muscle activities and result in greater spine loading.

Low back disorders are also associated with individual factors. Several personal or individual factors have been suspected of increasing the risk of LBD. Age appears to have some relationship to reporting of LBD [4, 10]. Worker strength is also associated with risk of LBD but only if linked to job requirements [52]. Trunk mobility has been identified as a significant factor in LBD but only when dynamic motion characteristics are considered [53-55]. Finally, smoking has been shown to be associated with a greater risk of low back disorder [56-58]. Recently, mismatches between personality characteristics and job demands have been shown to be associated with greater rates of musculoskeletal disorders [59]. Individual factors such as personality and gender have been shown to result in variations in muscle recruitment patters (coactivity) and differences in spine loadings [42, 51]. In addition, the experience of previous back injury has recently been shown to significantly increase trunk muscle coactivity and spine loading [60].

Is there a common link among these risk dimensions? It has been assumed that back pain is discogenic and has a mechanical origin [61]. Videman and associates [62] also confirmed the notion that LBD risk was associated with physically heavy work, such as MMH, by examining the functional spinal units of 86 cadavers whose work and LBD history were known. They found increased degeneration in the spines of those specimens who had performed physically heavy work. Hence, this suggests that occupationally-related LBDs are associated with spine loading. The previous discussion may, on the surface, appear to be contradictory, with some bodies of knowledge suggesting a causal relationship between physical work and LBD, other studies showing relationships between psychosocial factors and LBD, and still other bodies of literature suggesting that personal factors are responsible

for LBD. However, it is our view that physical factors, psychosocial workplace factors and individual factors combine to affect the risk of LBD risk. One has limited control over the manipulation of individual factors in the control of risk. However, one must understand the contribution of these individual factors to overall LBD risk if one is to appreciate the risk attributable to work that is above and beyond that due to the individual. Hence, one must work toward understanding how the various dimensions of risk combine to influence the overall risk of LBD.

Recently the National Academy of Sciences (National Research Council) [63] has developed a model that can help explain the interrelationship between the various dimensions that are suspected of leading to LBDs. Figure 1 portrays this logic graphically. At the heart of this model is a potential causal pathway to musculoskeletal disorders, such as LBD, that is related to a load–tolerance relationship of human tissue. The biomechanical system responds to workplace conditions through the systematic recruitment of muscles (co-activities) that result in the movements and the application of forces outside the body necessary to accomplish the work task at hand. These muscle co-contractions also result in the subsequent loading of the structures within the torso. If the internal loading exceed the tolerance of a tissue within the torso, the potential to stimulate pain receptors (nociceptors) and/or cause structural damage (vertebral end plate damage, disc damage, muscle strain, etc) exists and an injury can occur. Therefore, according to this logic, we can quantify "how much loading is too much loading" and thereby quantify risk.

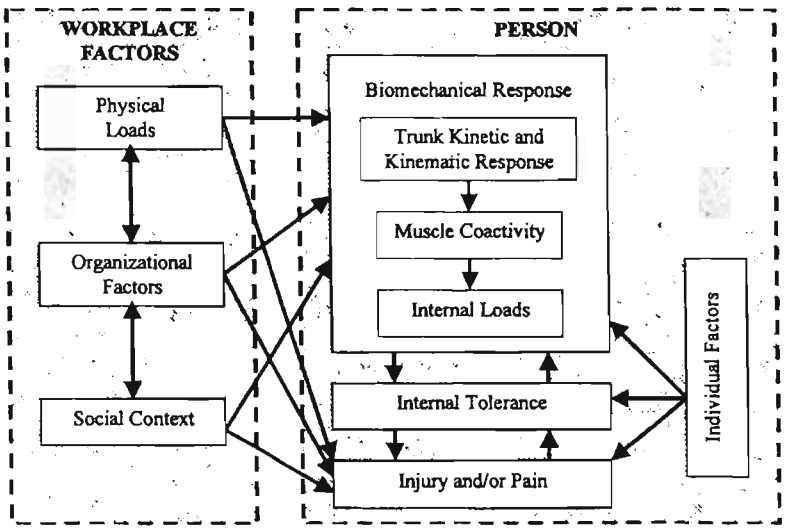

Figure 1. Conceptual model relating potential workplace risk factors to the development of low back pain (Adapted from NAS[63]).

As shown in Figure 1 the sequence of events involved in LBD can be influenced by individual factors as well as workplace factors. Factors unique to an individual (such as age, conditioning, personality, etc. [64-67]) can modify the coactivity response of the trunk muscles, affect the tissue tolerance (through altered tolerance or adaptation), and/or influence the outcomes of pain or injury. In a similar fashion, workplace factors can influence this injury pathway at various points in the sequence. Hence, physical loads imposed by the work (influenced by workplace design), organizational factors (such as pacing or overtime), and

social context (such as interpersonal relationships) all have the potential to influence the recruitment pattern of trunk muscles [21, 23-25, 27, 28, 33, 42, 68, 69]. These same factors are expected to also be able to influence tolerance and pain perception [70-78].

The project developed a method to estimated trunk muscle activity based on the premise that all risk dimensions influence the overall risk of LBD by affecting trunk muscle coactivity. The muscle coactivity allows us to understand the behavior of the trunk's musculoskeletal system and ultimately spine loads. The main objective of this work was to develop a Spine Loading Assessment System (SLAS) that has the capacity to quantify the influence of these various dimensions of risk upon the loading of the spine. This objective was achieved through the development of a Hybrid Neuro-Fuzzy Engine (HYNFE) system that has the capability of estimating the trunk muscle recruitment pattern in response to various physical and psychosocial workplace dimensions. This engine acts as the artificial "brain" to the SLAS by synthesizing information about the physical workplace, perceptions about the organizational and social climate, and individual modifiers and then estimating trunk muscle recruitment behavior. The engine is capable to interface with a well-developed electromyographic (EMG)-driven biomechanical model of the trunk in order to assess spine loading. As a result, the SLAS can accurately predict spine loading in the workplace in response to various risk factor dimensions without the need to collect EMG data in the workplace.

Completion of Specific Aims

This complete Spine Load Assessment System was developed by accomplishing the following specific aims:

1. Developed a multi-stage hybrid neuro-fuzzy "engine" (HYNFE) that is capable of accounting for musculoskeletal responses to physical load, psychosocial influences as well as individual characteristics when performing lifting tasks.

A complex engine was developed using fuzzy average with fuzzy cluster distribution techniques in combination with neural network structure. The neural and fuzzy approaches in the modeling of EMG activities were divided into two parts. In the first part, key input variables of the models were identified using a proposed fuzzy method called fuzzy average with fuzzy cluster distribution. In the second part, a neural network model was built to translate lifting task factors data into EMG signals under different task conditions. The ***model development section*** provides the background and process that occurred when developing the complex HYNFE.

2. Established and provided a large database necessary to "train" the HNFE.

While not all work conditions imaginable were incorporated into the training sets utilized to develop the HNFE, the boundaries of the data set encompasses the majority of lifting conditions found in the workplace. The section of ***Statistical Summary*** provides an overview of the data that makes up the database.

3. Developed user-friendly software that integrates the HYNFE with a well-developed EMG-assisted model so that one can compute spinal loads (SLAS development).

A software program has been established on the internet where researchers can upload the kinematic, kinetic, workplace conditions, and anthropometric variables to the website and the muscle activity of the ten trunk muscles. The muscle activity can then be entered into the user's EMG-assisted model so that spine loads can be estimated. The website also allows well-trained user (password required) to provide new data for further training of the HYNFE. The section called ***web-based software*** provides the link and description of the website that individuals can upload kinematic and kinetic data along with anthropometric data and have predictions of muscle activity for the ten trunk muscles.

4. Compared the SLAS-estimated spinal loads to EMG-assisted model spinal load predictions for a sample of typical conditions.

The current effort will establish the HYNFE primarily for physical workplace factor dimensions as well as for selected responses to psychosocial and personal factors where the data are available. The engine will have an open computational architecture so that future efforts can easily add to the engine's capacity and permit the model to consider more dimensions (e.g. the impact of previous experience) as our body of knowledge develops. A few examples are shown for several lifts that compare the measured EMG and the predicted EMG when input back into the EMG-assisted spine load model.

Methods

Model Development

Developing the HFYNFE to predict accurate and reliable EMG required a huge amount of previous collected data from a complex nonlinear system whose input-output relationship is not well understood. As a result, many factors influence the output of the system and need to be identified. So the first step to development was to identify which variables influenced the output of the system. As a result, any variables that had little or no influence on the output were removed from consideration and emphasis was put on the important variables. A method using fuzzy average with fuzzy cluster distribution was utilized to identify the key input variables for the purpose of reducing high dimensional input space as well as discovering the input-output relationship of the system. To avoid the interference of different distributions of the sampling data, the distribution of fuzzy clusters in the sampling data were identified. Fuzzy rule method and Fuzzy C-means method were used to partition the original sampling data set into fuzzy clusters. A new data set with the same distribution of the fuzzy clusters was then produced and the fuzzy average method was applied to it. By doing this, the interference from the distribution of the original sampling data was removed. In this manner, the method is straightforward and computationally easy.

After key variables have been identified, an EMG signal estimation model was built using a novel structure of feed forward neural network. The model estimated the full lifting motion at one time to obtain better accuracy of estimation compared to a point-to-point

estimation method. By using local connections for each lifting stage, the new architecture of the neural network incorporates both global and local features of the input data. The global connections "learn" the lifting process and determine the global trend of the estimated EMG curve, while the local connections concentrate on each phase of the motion and modify the estimation locally.

A basic structure of neural network designed for this problem is discussed. Then to overcome its drawbacks, a new structure was proposed and implemented.

Key Input Variables Identification Using FAFCD

Previous research has indicated variables such as trunk kinematics (angles, velocities, and accelerations) and trunk kinetics (moment) directly relate to the trunk muscle activity output. Furthermore, the differences between subjects' anthropometry also impact the EMG response through an interaction with the workplace and body dimensions. Mismatches between body dimensions and workplace layout can produce changes in both the kinematic and muscle activity response. With the extensiveness of potential variables for the HYNFE, variables with little influence on the EMG output were removed and more emphasis placed on the important ones. As a result, the model is more parsimonious and effective in predicting the muscle activities.

Basic Problem Statement of Model

For a nonlinear system with one output variable (muscle activity) and n associated input variables, m sampling data points were obtained. Each data point represented a joint measurement of all variables involved. The input data vectors are of such form:

$$\begin{bmatrix} \mathbf{x}_1 \\ \mathbf{x}_2 \\ \cdots \\ \mathbf{x}_n \end{bmatrix} = \begin{bmatrix} x_1^1 & x_1^2 & \cdots & x_1^m \\ x_2^1 & x_2^2 & \cdots & x_2^m \\ \cdots & & & \\ x_n^1 & x_n^2 & \cdots & x_n^m \end{bmatrix},$$

where x_i^j denotes the jth measurement of input variable x_i ($i=1, 2, \ldots n; j=1,2,\ldots,m$).

The output data vectors are of the following form:

$$\mathbf{y} = \begin{bmatrix} y^1 & y^2 & \cdots & y^m \end{bmatrix},$$

where y^j denotes the jth ($j=1,2,\ldots,m$) measurement of the output variable y.

From the above sampling data of input-output pairs, the relationship between each input variable and the output variable was found. The difficulty of finding x_i-y relationship resides in that the change of y is caused by the joint influence of all the input variables, instead of only the influence of x_i.

Related Work and Limitations

The general problem at hand has broad applicability with many researchers adopting various methods. Bartlett and associates [79] uses a neural network method. During training, the algorithm automatically constructed the appropriate artificial neural network (ANN) architecture. The importance of each input variable was provided as a by-product. However, there are a couple of limitations with this method including: 1) inability to determine how each input variable affects the output and 2) different neural networks development is time consuming.

Yuan and Klir [80] used the full class of Mahalanobis distances to search by an evolutionary algorithm for the optimal distance—one under which the fuzzy c-means algorithm produces a fuzzy partition of the given data set that is as close as possible to the given crisp partition. The contribution of each variable to this partition was then inferred from parameter values of the optimal Mahalanobis distance. This method employed evolutionary computation. However, the method is computationally intensive and obtaining specific results is not straightforward. Furthermore, the method fails to provide information about the relationship between input and output variables.

Sugeno and Yasukawa [81] proposed an iterative algorithm for the input identification. Different models were generated to search for the optimal combination of variables. The total number of combinations was 2^n-1, where n was the number of input variables. For a high dimensional system with many input variables, the number of needed models is enormous.

Chiu and associates [82] used a backward selection procedure that starts with all possible variables and reduces one variable at each stage. Premises in the fuzzy rules of an initial model were systematically removed to search for the best simplified model, without generating new models. But after the iteration process of searching, different results were obtained when three different criteria for model selection were used followed by a Takagi-Sugeno type model that was generated for each solution. The final model selection was based on the comparison of the model errors, which makes the method complicated and time consuming.

Lin and associates [83, 84] proposed a "fuzzy curves" method. For each input variable x_i, the m data points are plotted in the x_i - y space. A fuzzy rule was defined according to each sampling data point (x_i^j, y^j) $(i=1,2,...,n, j=1,2,...,m)$ in the following form:

$$R_i^j: \text{IF } x_i \text{ is } \mu_{ij}(x_i) \text{ THEN } y \text{ is } y^j,$$

where $\mu_{ij}(x_i)$ is a Gaussian membership function of x_i.

A "fuzzy curve" was produced by using a defuzzification method, which stands for the x_i - y relationship. The importance of the input variables was ranked according to the ranges covered by the fuzzy curves. The fuzzy curve method was computationally easy. Lin and associates [83] used this method in fuzzy-neural system modeling to determine model structure and set the initial weights in the model. The method was also used in many other

papers [84-92]. Lin et al. [84] utilized the method to eliminate spurious or dependent inputs. Azeem and associates [85] utilized the method to set the initial parameters of the neuro-fuzzy model. Morabito and Versaci [86] used the method to rank the input variables and determine the optimal rules by describing the behavior of the system. Papadakis and associates [87] adopted the method to generate fuzzy models for short term load forecasting.

The usage of this method for the EMG signal estimation system for manual lifting tasks was found to be more difficult due to the large distribution of the data set. In other words, the influence of the input variables obtained from this method may vary from sample to sample. For a stable system, this should not happen. In most cases, the influence of each input variable is an inherent property of the system, regardless of the distribution of sampling data. Based on this limitation, the method was improved by introducing the FAFCD method.

As mentioned in the prior section, in the method of fuzzy curves, a fuzzy rule was defined according to each sampling data point (x_i^j, y^j). From m data points, m fuzzy rules were obtained. The fuzzy membership functions for input variable x_i are Gaussian membership functions centered at x_i^j:

$$\mu_{ij}(x_i) = \exp(-(\frac{x_i - \overline{x}_i^j}{\sigma})^2)$$

where $\overline{x}_i^j$ and σ are the center and width of the membership function, respectively.

Then, the fuzzy curves are produced from defuzzification:

$$C_i(x_i) = \frac{\sum_{j=1}^{m} y^j \mu_{ij}(x_i)}{\sum_{j=1}^{m} \mu_{ij}(x_i)}$$

Lin and associates [83] demonstrated and validated this method using a nonlinear system defined as:

$$y = (2 + x_1^{1.5} - 1.5\sin(3x_2))^2, 0 \leq x_1, x_2 \leq 3$$

where x_1 and x_2 are two input variables, y is the output variable.

Here, the defuzzified curves of y in x_1 - y and x_2 - y space are plotted in Figure 2 (A) and (B), respectively. The sample data were generated using the system function above, with x_1 and x_2 uniformly distributed in the interval [0 to 3] (Figure 2 (C)). R in the figure is the ratio of the range of y covered by the curve to the whole range of y. The value of R represents the influence of the corresponding input variable, instead of using the ranges covered by the fuzzy curves as in Lin et al. [83].

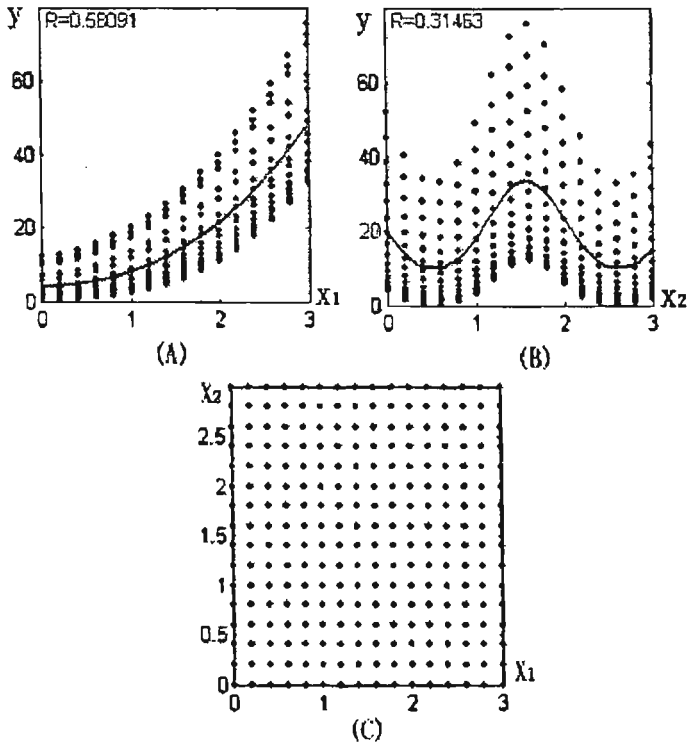

Figure 2 (A): The x1- y relationship from defuzzification. (B) The x2-y relationship from defuzzification. (C) The distribution of inputs x1 and x2

curves must still work when the distribution of the sample data changes. Figure 3 (A) gives us a different result of x_2 - y relationship when the data were generated with *x1* and *x2* shown in Figure 3 (B). If the sampling data were not uniformly distributed, the curves were distorted. This example shows that the fuzzy curve method puts restrictions on the distribution of sampling data. A short discussion of this point will be provided with a new approach derived.

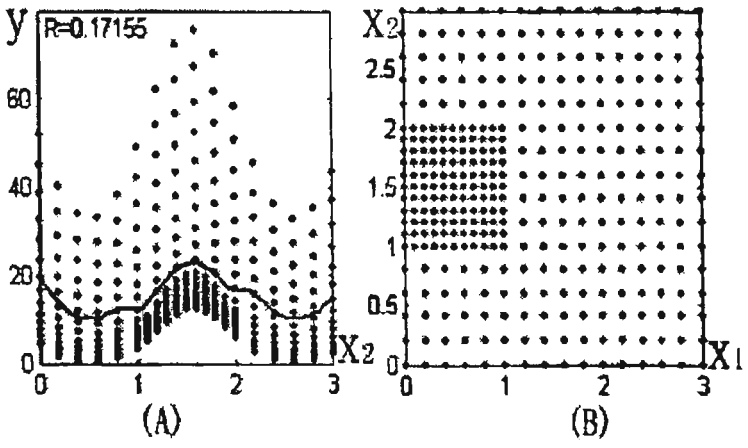

Figure 3: (A) The x2 - y relationship from defuzzification. (B) The distribution of inputs

As stated before, the importance of the input variables were ranked according to the ratio of the range of y covered by the curve produced from defuzzification to the whole range of y. The ratio, Influence Rate (R), for the input variable x_i was defined by the following equation:

$$R_{x_i} = \frac{C_i(x_i^u) - C_i(x_i^l)}{a}$$

where $C_i(x_i^u)$ is the highest point on the curve, $C_i(x_i^l)$ is the lowest point on the curve, and a is the whole range of y.

$C_i(x_i^u)$ and $C_i(x_i^l)$ were calculated from defuzzification. The membership of each value of x_i to all the m membership functions was calculated. The width of the Gaussian membership function was taken as about 20% of the length of the input interval of x_i. If the width σ was very small, only those membership functions with a center (mean of the Gaussian function) close to current value of x_i had a significant value, while the membership functions far from it had a value close to zero. When σ approaches zero, only those membership functions with their centers equal to x_i^u and x_i^l need to be taken into account.

$$R_{x_i}(\sigma \to 0) = \lim_{\sigma \to 0}\left(\frac{C_i(x_i^u) - C_i(x_i^l)}{a}\right)$$

$$R_{x_i}(\sigma \to 0) = \frac{1}{a} \times \lim_{\sigma \to 0}\left[\frac{\sum_{j=1}^{m} y^j \mu_{ij}(x_i^u)}{\sum_{j=1}^{m} \mu_{ij}(x_i^u)} - \frac{\sum_{j=1}^{m} y^j \mu_{ij}(x_i^l)}{\sum_{j=1}^{m} \mu_{ij}(x_i^l)}\right]$$

$$= \frac{1}{a} \times \lim_{\sigma \to 0}\left[\frac{\sum_{j=1}^{m} y^j \exp(-(\frac{x_i^u - \bar{x}_i^j}{\sigma})^2)}{\sum_{j=1}^{m} \exp(-(\frac{x_i^u - \bar{x}_i^j}{\sigma})^2)} - \frac{\sum_{j=1}^{m} y^j \exp(-(\frac{x_i^l - \bar{x}_i^j}{\sigma})^2)}{\sum_{j=1}^{m} \exp(-(\frac{x_i^l - \bar{x}_i^j}{\sigma})^2)}\right]$$

The memberships of x_i^u and x_i^l to other membership functions were zero. Suppose there are s membership functions with a center equal to x_i^u and h membership functions with a center equal to x_i^l, then the above function becomes:

$$R_{x_i}(\sigma \to 0) = \frac{1}{a} \times \left(\frac{\sum_{k=1}^{s} y_k^u}{s} - \frac{\sum_{k=1}^{h} y_k^l}{h}\right)$$

where y_k^u $(k= 1,2,...,s)$ are the values of y when $u_{ij}(x_i^u)=1$; and y_k^l $(k= 1,2,...,h)$ are the values of y when $u_{ij}(x_i^l)=1$.

The above formula indicates that the range of the curve (when σ approaches zero) is the difference between the average value of y at $x_i=x_i^u$ and the average value of y at $x_i=x_i^l$. If σ is not approaching zero, the value of C_{xi} at $x_i=x_i^u$ takes those data points around $x_i=x_i^u$ into account, but it is still a weighted average. Since it has a meaning of average carried in a fuzzy sense, we call it Fuzzy Average.

After expressing the value of the defuzzified curve for x_i at $x_i=x_i^u$ as a weighted average which takes the points around $x_i=x_i^u$ into account, the next step was to find out what

determines the value of this average. For simplicity, the condition when σ approaches zero is still considered. In this condition, the value of the fuzzy average at $x_i=x_i^u$ is the arithmetical average of y at $x_i=x_i^u$:

$$C_i(x_i = x_i^u) = \frac{\sum_{k=1}^{s} y_k^u}{s}$$

$C_i(x_i=x_i^u)$ is the fuzzy average value of y at $x_i=x_i^u$ in the x_i-y space. The value of $C_i(x_i=x_i^u)$ depends on the values of y at $x_i=x_i^u$ (the values of y_k^u). The values of y_k^u are decided by both the system function and the values of the input variables.

Let's define the system function of a MISO system as

$$\mathbf{y} = f_s(x_1, x_2, \ldots, x_n) = f_s(\mathbf{x})$$

where f_s is the system function and y is the output vector;

Therefore the average value of y at $x_i=x_i^u$ in the x_i-y space is

$$C_i(x_i = x_i^u) = \frac{\sum_{k=1}^{s} f_s(x_1^k, x_2^k, \ldots, x_n^k)}{s}$$

where $k=1,2,\ldots,s$, assuming s data points at $x_i=x_i^u$.

For easier notation, the fuzzy average of y in the x_i-y space is considered. Using $x_{(2-n)}$ to represent $[x_2, x_3, \ldots, x_n]$, the fuzzy average of y in the x_1-y space becomes

$$C_1(x_1) = \frac{\sum_{k=1}^{t} f_s(x_1, \mathbf{x}_{(2-n)}^k)}{t}$$

where t is the number of data points at each value of x_1 (they are not the same for different values of x_1). Then it can be found that only when vectors $x^k{}_{(2-n)}$ ($k=1,2,\ldots, t$) are the same for all x_1, $C_1(x_1)$ is determined only by x_1, so that the above function can reflect the x_1-y relationship. Otherwise $C_1(x_1)$ is determined by all the input variables, therefore can not reflect the relationship between x_1 and y.

Figure 2 is the 2-dimensional example with two input variables x_1 and x_2, in which x_1 have the same values at each value of x_2 (Figure 2 (C)). The fuzzy average of y in the x_2-y space reflects the x_2-y relationship correctly. While in Figure 3, x_1 does not have the same values at each value of x_2, so the fuzzy average of y can not correctly reflect the x_2-y relationship.

Thus, to find out the x_i - y relationship using fuzzy average method, each of the input variables should have the same values along the axis of x_i, respectively. For the real world data, this requirement is oftentimes difficult to meet. While for the 2-input example, if many sampling data points spread all the range of x_1, the fuzzy average of y in x_2 - y space can

reflect the x_2 - y relationship as long as x_1 has roughly the same distribution at any value of x_2. Figure 4 shows the result of this condition. In Figure 4 (B), x_1 was generated randomly using Matlab command "rand" with *uniform* distribution. It shows that fuzzy average method works in this situation (Figure 4 (A)).

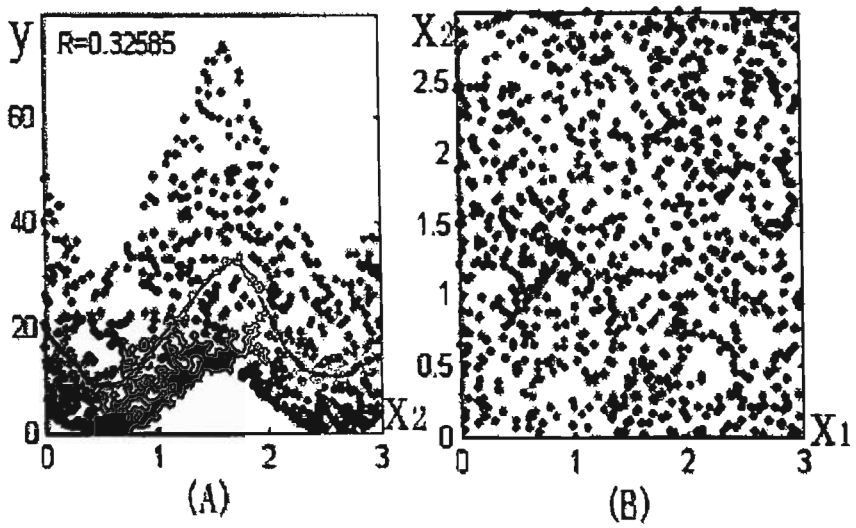

Figure 4. (A) The x2 - y relationship from defuzzification. (B) The distribution of inputs

For many practical applications, it can not be assumed that each input variable (except x_i) has the same distribution along x_i axis, respectively. This means for a certain system, if different sampling data sets are used, the fuzzy average may be different. Then, the conclusion for the importance of input variables may be different. This required pre-processing of the sampling data set to transform to a similar distribution set.

Improved Method

Using fuzzy average method, the significance of variable x_i can be correctly evaluated without the interference of other input variables only when all other input variables have the same distribution along x_i axis. To transform the sampling data set into this form, fuzzy clustering is considered to change the distribution of the data set. Again, the example of the system with two input variables x_1 and x_2 shown in Figure 2 is used.

Suppose more data points fall into a small region than into other regions in the x_1 - x_2 spaces (as in Figure 3 (B)). Fuzzy clustering method is used to divide the data points into groups. The number of data points in each group (fuzzy cluster) will be different since the distribution of the data is uneven. If one data point (for instance, the fuzzy cluster center) is used to represent each group, a new data set with the distribution of fuzzy clusters can be obtained. Since different number of sampling data in small regions will be replaced by the same number of cluster center, a new data set with better distribution may be obtained. The Fuzzy C-means method (discussed below) was used to cluster the data. After a short discussion of the limitations of the method, an improved method is proposed.

Each of the data points represents a point in the n-dimensional Euclidean space (n is the input dimension). The purpose of clustering was to partition the data set into clusters in such a way that data points in each cluster were highly similar to each other, while data points assigned to different clusters had low degrees of similarity.

Fuzzy c-means (FCM) allows one data point to belong to two or more clusters [93, 94]. It provides a method that group data points in multi-dimensional space into a specific number of clusters. It is based on minimization of the following objective function:

$$J_m = \sum_{i=1}^{N} \sum_{j=1}^{C} \mu_{ij}^{m} \parallel x_i - b_j) \parallel$$

where m is the number of clusters, u_{ij} is the degree of membership of x_i in the cluster j, x_i is the ith of n-dimensional measured data, b_j is the n-dimension center of the cluster, and ||*|| is a norm expressing the distance between measured data and cluster center.

FCM is first used to cluster the data shown in Figure 3 (B). For this method, the number of clusters needs to be predefined. In this example, the number of clusters was taken as 50. Next, the method produced 50 centers of the clusters that were used to form a new data set. After this process, the distribution of the obtained new data set is shown in Figure 5. The crosses are the original data points and the circles are the centers of the clusters.

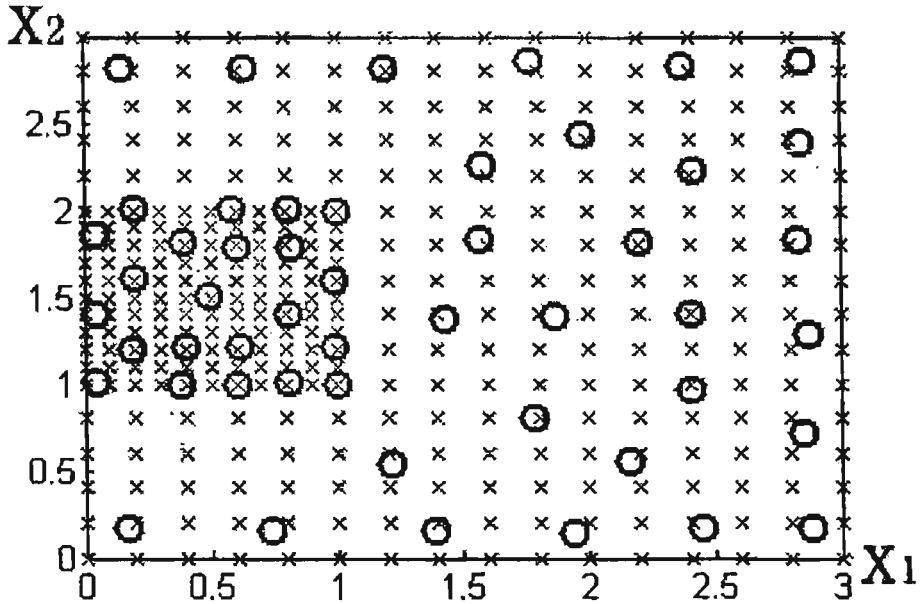

Figure 5. Clusters generated using FCM. ``X" is the original data point; ``O" is the fuzzy cluster center.

It can be seen that the distribution of the data did not change. It is important to understand why the FCM does not change the distribution. The reasoning behind the consistency of the distribution is based on the iteration process of FCM where the membership is updated though

$$\mu_{ij} = \left[\sum_{k=1}^{C} \left(\frac{\| x_i - c_j) \|}{\| x_i - c_k) \|} \right)^{\frac{2}{m-1}} \right]^{-1}$$

and the cluster centers are updated though

$$b_j = \frac{\sum_{i=1}^{N} x_i \cdot \mu_{ij}^m}{\sum_{i=1}^{N} \mu_{ij}^m}$$

The membership and the cluster centers are updated to minimize the total weighted distance between data points and the cluster centers of the fuzzy partition. Thus, in areas where more data points exist, there are more cluster centers in order to make the total weighted distance between all data points and the cluster centers smaller. Therefore, the data distribution remains the same when using FCM.

To generate even cluster distributions, the input space must be partitioned using fuzzy rules before applying FCM. The following steps were undertaken: 1) a fuzzy rule base was built for the nonlinear system, 2) those data points that excited a particular fuzzy rule with high firing strength were grouped to the same partition. The fuzzy rule base is in the form of

IF x_1 is A_{11} and x_2 is A_{21} and ... and x_n is A_{n1} THEN y is y^1

IF x_1 is A_{12} and x_2 is A_{22} and ... and x_n is A_{n2} THEN y is y^2

...

IF x_1 is A_{1m} and x_2 is A_{2m} and ... and x_n is A_{nm} THEN y is y^m

where A_{ij} *(i=1,2,...,n; j=1,2,...,m)* and y_j are fuzzy sets of x_i and y, respectively.

The fuzzy partitions generated by the fuzzy rules are shown in Figure 6. If the width σ' of Gaussian membership function is the same for all the fuzzy sets, the partition is an even partition.

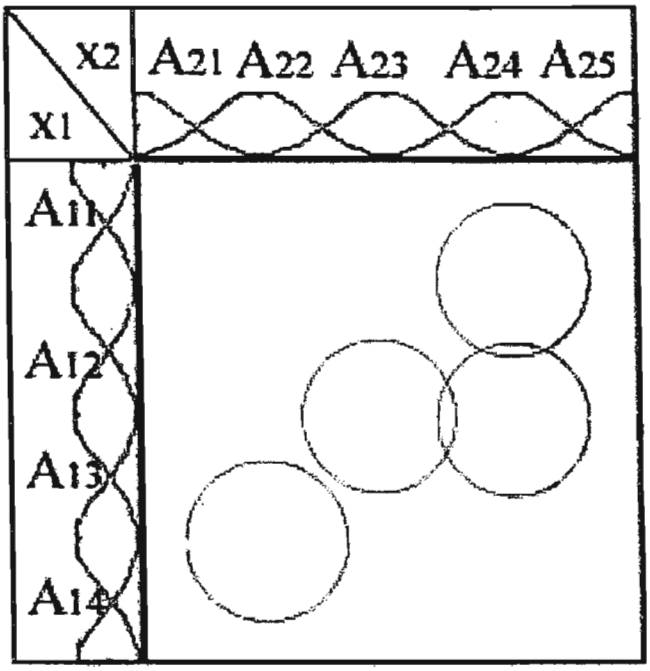

Figure 6: Partitions generated by fuzzy rules (with fixed width σ')

The method is implemented as follows: the first sampling data point is taken as center of a cluster and a corresponding fuzzy rule is built. The parameters are chosen as follows:

$$\overline{x}_i^j = x_i^j$$

$$\sigma' = \frac{1}{30} \times d$$

where d is the range of the input variables (normalized to the same range).

For every sampling data point, the firing strength (degree of fulfillment) of each existing rule is calculated:

$$G_j = \prod_{i=1}^{n} (\mu_{ij}(x_i)) = \prod_{i=1}^{n} \exp(-(\frac{x_i - \overline{x}_i^j}{\sigma'})^2)$$

AND operation is used here.

If the firing strength

$$G_j \geq \beta,$$

then the sampling data point is close to the data points in the partition. Thus, it belongs to this partition. β is a predefined threshold as the least acceptable degree and determines the extent of the similarity to be classified into the partition. If the firing strength is less than the threshold β, then a new fuzzy rule (a new partition) was created.

After all the data are partitioned, FCM algorithm was used to cluster data points in each small partition. The same number of clusters was set for each small partition so that the distribution was consistent. In some cases when the partition was small enough, only one cluster was set for each partition with the center found by FCM. Using the centers of the clusters to represent the clusters is preferred method. But for real world systems, the corresponding output of the system to the centers are not always available which leads to the centers to being not concurrent to the existing data points. So, the sampling data points closest to the center of a cluster were used to represent the cluster. The closest data point was decided by its Euclidean distance to the center.

$$\mathbf{x}_{closest} = \| \mathbf{x}_i - \mathbf{x}_{center} \|_{min}$$

There was a loss of information during this process, but the number of partitions can be controlled to make sure only redundant data points were removed while keeping enough data points to represent the complete original data set in the input space. This was done by adjusting σ'. If σ' approaches 0, then each sampling data point is a partition; if σ' approaches infinity, only one partition exist.

When only one cluster is set for each partition, the number of clusters is the same as the number of partitions. So if σ' is too small, the distribution may not change and the number of clusters will be large; if it is too big, some clusters with less data points may be combined into other clusters and its representation is lost when only the cluster center is kept. Normally σ' is taken as 1/30 of the range of the normalized input variables. This partitions the input space into many small partitions which can represent the input space adequately, and at the same time remove redundant sampling data points inside the small partitions. The procedure of FAFCD is shown in Figure 7.

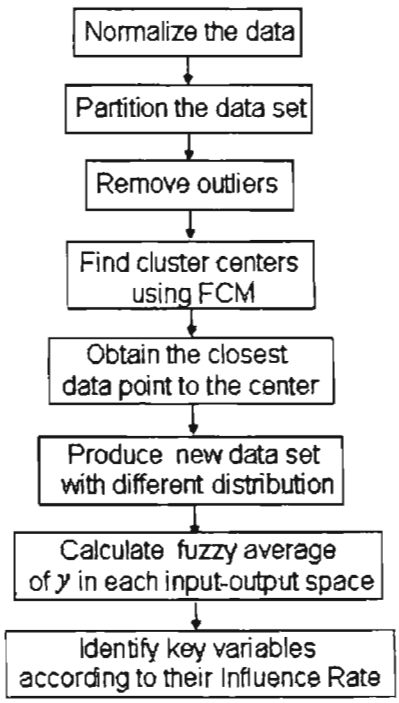

Figure 7. Procedure for fuzzy average with fuzzy cluster distribution (FAFCD)

Distribution of the data in Figure 3 (B) became more even after being processed by the above method (see Figure 8 (B)). Hence, the fuzzy average of y in x_2 - y space can reflect the x_2 - y relationship more accurately (Figure 8 (A). These results are very similar to the results generated in Fig. 1, which is a uniform distribution.

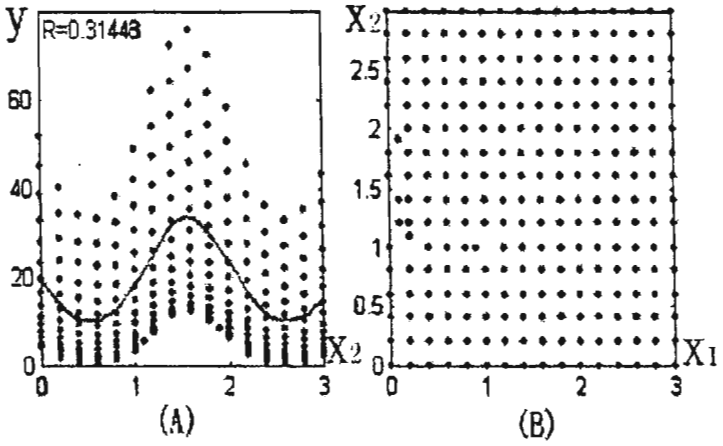

Figure 8: Results using fuzzy average with fuzzy cluster distribution (FAFCD). (A) The x_2 - y relationship from defuzzification. (B) The distribution of inputs.

Other Considerations to the Improved Method

Some considerations and improvements were implemented to further improve the method. Before applying FAFCD, the data set was preprocessed. Because different variables are measured in different units and with different numerical ranges, a bias may be introduced to the process. Thus, the data need to be normalized:

$$\widetilde{x}_i^j = \frac{x_i^j - (x_i^j)_{min}}{(x_i^j)_{max} - (x_i^j)_{min}}$$

where $\widetilde{x}_i^j$ is the value after normalization; x_i^j is the data to be normalized; $(x_i^j)_{min}$ is the minimum value of vector x_i; $(x_i^j)_{max}$ is the maximum value of vector x_i.

When using the fuzzy average method, all the existing membership functions μ_{ij} for each value of x_i were calculated. If the center of a membership function ($\overline{x}_i^j$) is far away from the current value of x_i, the value of the membership function becomes very small and has no much influence on the fuzzy average value. For instance, when $x_i - \overline{x}_i^j = 3\sigma$, the value of the membership function is very small:

$$\mu_{ij}(x_i) = \exp(-(\frac{3\sigma}{\sigma})^2) = \exp(-9) = 1.23e-4$$

Therefore only the membership functions whose centers are in the range of 3σ need to be calculated. The values of the other membership functions were very small and were neglected. This can reduce the number of membership functions to be calculated. For the example used in the simulation section, there are 29,880 data points, which means for each value of x_i, 29,880 membership functions need to be calculated. If only the membership functions whose centers are in the range of 3σ are calculated, this number can be reduced to 1/10 of the total number of membership functions. So the fuzzy average can be calculated much faster with almost no quality decrease.

During our clustering process, outliers often became individual clusters. When the cluster center was used to form a new data set, the outliers were kept. If the sampling data set had a large number of data points, those clusters that contained very few data points (predefined by a threshold) were removed. Outliers were normally removed by this method. The threshold was determined according to the total number of data points.

EMG Estimation Using A Neural Network Model

Since there is strong relationship between lifting task factors and EMG activity, models can be built to simulate the relationship by predicting one from the other variable. Many studies concentrated on predicting torque or kinematics from EMG [95-97], whereas predicting EMG from kinematics variables has seldom been done. Here a model that uses kinematics (and other variables) as input to predict the EMG signals was built.

As stated before, the muscle activities during manual lifting are influenced by multiple variables including individual (e.g. anthropometry, gender, and personality) and workplace (e.g. physical and psychosocial) factors. The indeterminate characteristics of muscle recruitment cause the relationships between task factors and muscular activities to be complex with a certain level of variability. Therefore, the relations between EMG data and lifting-related variables are not easily formulated with the traditional mathematical forms because they are often too complex to define [98]. Since the exact relationship between the multiple input variables and EMG signal was not clear, finding the transfer function between them was difficult. Neural networks extract the implicit nonlinear relationship between the signals by learning from training data, which makes it a good method for building the kinematics - EMG model. Neural networks have previously demonstrated advantages in many biomedical applications. By building a neural network model, establishing a complex mathematical model to express the muscle activation dynamics can be avoided.

A basic neural network model was constructed initially. To overcome its drawbacks and provide better performance with respect to accuracy and consistency, an improved neural network model with novel architecture was developed.

Basic Neural Network Model

For the problem described above, a basic feed forward neural network model with one hidden layer was built. This model had input variables including kinematic and kinetic variables as well as individual variables. The outputs were normalized EMG signals of ten

trunk muscles. The input/output variables are listed in the simulation section.

In this basic model, the EMG signals are predicted point by point. Each input vector consists of 9 kinematic and 3 kinetic variables with one sampling data point for one subject, as well as the four subject antropometric variables. The kinematics variables are time series, while the subject variables single values measurements. All sampling points of all subjects in a same motion were used to train the network one by one. After training by back-propagation algorithm, the performance of the neural network model was tested on an evaluation data set. According to these initial results, this model did not provide good estimation performance.

Thus, the model was limited in the ability to estimate the EMG activity which resulted from the nature of muscular activities. The activity of one muscle is a complex response to many factors and is often affected by the activities of other muscles. Therefore, if the joint's status is changed along with the body posture, the level of the EMG signals is also changed but may not be completely uniform. From the origin of the lift to the destination, there were typical patterns with a certain level of variability throughout the motion which resulted in different muscle activation levels. The model evaluated EMG at each time point one by one using the same network, which does not account for the change of the lifting process and the influence of other motions. The generalization ability of the model is thus decreased.

Improved Neural Network Model

The unsatisfactory performance of the conventional network model stated above shows that predicting point by point was not be a good idea. After all, the whole motion is being modeled. A better approach might be better to estimate the entire span of motion at one time. Therefore, another network with all the sampling data points of a lift motion as one whole input vector was built. The outputs were EMG data of ten muscles of the whole lift motion.

The structure of the new model is shown in Figure 12. The solid connections which are called "global connections" form a fully connected feed forward neural network with two hidden layers. The dotted connections are "local connections" which only connect the input neurons and output neurons belonging to the same sampling data point. Local connections of the first sampling data point are enclosed in the dashed rectangle. The white "neurons" in the figure are hidden neurons of the local connections. The darkest "neurons" stand for the subject variables.

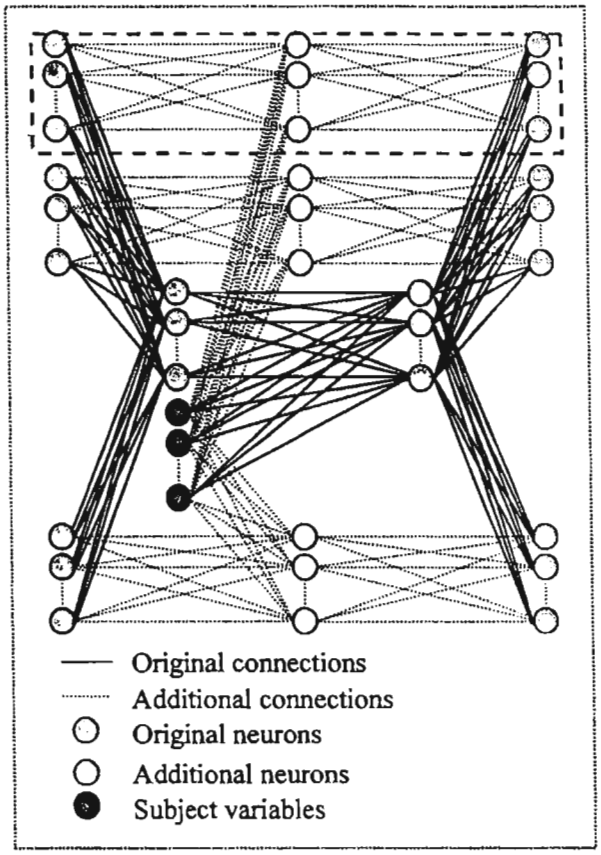

Figure 12: The neural network structure with local connections

Characteristics of the Model Structure

In this model, each training example was the whole motion of a subject and the outputs were the EMG signals during the whole motion. This makes the problem straightforward and easy to compute. More importantly, this model accounted for the influence between motions and the interactions between muscles. These were global features that could not be extracted from isolated sampling points.

In the previous basic model (described above), the input-output pairs were independent points. When the data of one sampling point were fed into the network, the behavior of the muscles before and after this point was unavailable to the network. But when the data of the whole motion were fed into the network, such time dependent information was included. As stated before, the generalization ability of the previous basic model was decreased because it evaluates EMG at each time point one by one using the same network. While in the improved model, the local connections were established for each sampling data point respectively. Thus, the model decomposed the input space (the whole lift process) in temporal domain and learned the different phases of the motion separately, so that the generalization ability can be improved. Also, since the input and output neurons are only connected when they belong to the same sampling point, this model has a better "locality". When the values in a small area of the input space changed, it will only influence the output of the corresponding small area, without significantly interfering with the values outside this small area.

The global connections (solid connections) have two hidden layers, with 25 hidden units in each layer. If the subject variables are connected to the first hidden layer similar to the kinematic and kinetic variables, the network will be insensitive to subject variables. Because of the existence of a large number of inputs, the importance of subject variables will be decreased. To increase the importance of subject variables, they are connected directly to the second hidden layer of the global connections [99].

Comparison with Modular Neural Networks

As described above, the structure of the model contains global connections and local connections. The local connections extracted the relationships among local inputs, for each sampling data point. If local connections for each sampling data point was taken as a module (as indicated by a dashed rectangle in Figure 12), then this architecture has some similarities to the modular neural networks. In a modular neural network, a module is a sub-network which is trained independently in parallel with other sub-networks, using a particular feature subset. The outputs of these sub-networks are mediated by a higher level neural network on the top of the individual networks (an integrating unit or gating network) [100-102].

Modular neural network decomposes complicated task in feature or temporal domain. Optimal solutions for all subtasks are obtained separately and the overall output will be based on them. Modular neural networks have been used in many applications and demonstrated advantages in some aspects over existing methods based on traditional neural networks [103-105]. Khotanzad et al. [103] developed a modular neural network that was based on a hourly load forecaster. The behavior of the load was decomposed into three distinct trends which were learned by several feed forward sub-networks. The forecasts produced by each module were then combined by adaptive filters to obtain the final forecast. Lu and associates [104] developed a method for classifying single-trial electroencephalogram (EEG) signals using min-max modular neural networks. The complex EEG classification problem was divided into a number of sub-problems which were learned by individual smaller network modules in parallel. A large set of high-dimensional EEG data can be learned efficiently using this method. Jacobs and Jordan [105] developed a modular neural network that learns to perform control tasks using a piecewise control strategy. The plant's parameter space was partitioned into a number of regions, and a different network learns a control law in each region. Simulations revealed the performance was superior to that of a SNN on a multi-payload robot motion control task. Based on the above applications, it can be seen that the major advantages of modular neural networks are as follows: 1) the decomposition of input space makes it easier to deal with complex and large-scale problems, 2) better generalization performance can be achieved because learning subtasks using sub-networks is easier than learning a complex task, and 3) the MNN is more robust since the failure of one sub-network does not mean that all of the sub-networks fail to do so.

Both modular neural networks and the current model decomposed the complicated task in feature or temporal domain, therefore divided it into several subtasks. The "modules" were trained in parallel on a subset of data. The modules specialize in learning features of different regions of the input space.

The differences between the current model and the modular neural networks resided in the relationship between the modules and the integrating network. The modular neural network, as defined by Haykin [106], was one in which the computations performed by the network were decomposed into two or more subsystems that operate on distinct inputs without communicating with each other. The outputs of the modules were mediated by an integrated unit that is not permitted to feed information back to the modules [107]. In the current model, although the local connections operated in parallel, they were related through the global connections. The global connections were trained simultaneously with the local connections and were considered in the weight adjusting. Thus the global connections performed a different function from the gating network in modular neural networks.

There are two types of modular neural networks: 1) mixture of experts modular network (MEMN) which has decomposition of data and 2) committee of networks modular network (CNMN) which has decomposition of features [109, 110]. The output of MEMN can be represented by a linear combination of outputs of several distinct functions:

$$o(m) = \sum_{k=1}^{K} \pi_k f_{k,m}(x_k)$$

where $0 \leq \pi_k \leq 1 k = 1, 2, \ldots . K, \sum_{k=1}^{K} \pi_k = 1$

The functions $f_{k,m}(x_k)$ are mixing components which represent expert networks. The parameters π_k are mixing weights which are the outputs of the gating network, k is a label representing an individual neural network, and m is a class label. The output of CNMN can be an average of outputs of several distinct functions

$$o(m) = \frac{1}{K} \sum_{k=1}^{K} f_{k,m}(x_k)$$

where x_k is the subset of the feature vector which is applied to network k.

For the current model, the output was expressed as

$$o(p) = f\left(v_{pql_1}^{(G)}, v_{qml_2}^{(G)}, w_{mn}^{(G)}, v_{ij(r)}^{(L)}, w_{jk(r)}^{(L)}, x_p\right)$$

where x_p is the input of the model. $v_{pql_1}^{(G)}$ and $v_{qml_2}^{(G)}$ are weights in the first and second hidden layer of global connections, respectively, $w_{mn}^{(G)}$ are $w_{jk(r)}^{(L)}$ weights in the output layer of global connections and local connections, respectively, $v_{ij(r)}^{(L)}$ are weights in the hidden layer of local connections, *(G)* and *(L)* stand for the global connections and local connections, respectively. l_1 and l_2 stand for the first and second hidden layer, respectively, *(r)* stands for the rth sampling data point. p, q, m, n, i, j, k stand for neurons in different layers, and f denotes the nonlinear function representing the neural network.

In modular neural network, the modules are complete stand-alone neural networks. The training of modules is separate and independent from the integrating unit, while in the current model, the training of local connections and global connections were related and inseparable. They both participated and contributed to the weights adjusting of the whole network. Furthermore, in modular neural network, the final output of the system is based on outputs of the modules. The gating network decided how the outputs of the modules should be combined to form the final output, while the global connections in the current model were integrated with local connections. They were not mediating the outputs of local connections, but contributed to the overall output as the local connections do.

Training Algorithm of the Current Model

Output of the first hidden layer of the global connections were expressed as:

$$y_{ql_1}^{(G)} = f^h(net_{ql_1}^{(G)}) = f^h(\sum v_{pql_1}^{(G)} x_p^{(G)})$$

in which $v_{pql_1}^{(G)}$ is the weight of connection between the pth input neuron and the qth first hidden layer neuron, $x_p^{(G)}$ is the pth input of the global connections (it contains all the sampling points), and f^h is the activation function of hidden layers.

Output of the second hidden layer was expressed as:

$$y_{ml_2}^{(G)} = f^h(net_{ml_2}^{(G)}) = f^h(\sum v_{qml_2}^{(G)} y_{ql_1}^{(G)})$$

in which $y_{ml_2}^{(G)}$ is the weight of connection between the qth first hidden layer neuron, the mth second hidden layer neuron (note: input of the second hidden layer consists of output of the first hidden layer and subject variables connected directly to the second hidden layer), and l_2 stands for the second hidden layer.

Then the scalar product of $y_{ml_2}^{(G)}$ and the weights was calculated:

$$net_n^{(G)} = \sum_m w_{mn}^{(G)} y_{ml_2}^{(G)}$$

$w_{mn}^{(G)}$ is the weight of connection between the mth second hidden layer neuron and the nth output layer neuron of the global connections.

Similar to the above, the forward pass of local connections was as follows. Output of the hidden layer of local connections was expressed as:

$$y_{j(r)}^{(L)} = f^h(net_{j(r)}^{(L)}) = f^h(\sum_i v_{ij(r)}^{(L)} x_{i(r)}^{(L)})$$

in which $x_{i(r)}^{(L)}$ is the ith input of the rth sampling data point's local connections.

The scalar product of $y_{j(r)}^{(L)}$ and the weights was

$$net_{k(r)}^{(L)} = \sum_{j} w_{jk(r)}^{(L)} y_{j(r)}^{(L)}.$$

$w_{jk(r)}^{(L)}$ is the weight of connection between the *j*th hidden layer neuron and the *k*th output layer neuron of the *r*th sampling data point's local connections.

Then, the neurons of the output layer of the whole network were combined the outputs of both the global connections and the local connections:

$$net_{k(r)}^{(C)} = net_{k(r)}^{(L)} + net_{k(r)}^{(G)}.$$

$$o^{(C)} = f^{o}(net^{(C)})$$

(C) here means "combined". f^{o} is the activation function of the output layer.

Backward pass of the *r*th sampling data point's local connections was computed as follows.

The error function to be minimized was

$$E_{(r)} = \frac{1}{2}\sum_{k=1}^{K}(d_{k(r)} - o_{k(r)})^2$$

$d_{k(r)}$ and $o_{k(r)}$ are the actual and estimated output of the *r*th sampling data point, respectively. $o_{k(r)}$ is part of the whole output (the full lift motion).

Weight adjustment for the output layer was calculated by:

$$\begin{aligned} w_{jk(r)}^{(L)}(t+1) &= w_{jk(r)}^{(L)}(t) - \eta^{(L)} \frac{\partial E_{(r)}}{\partial w_{jk(r)}^{(L)}(t)} \\ &= w_{jk(r)}^{(L)}(t) - \eta^{(L)}(o_k - d_k)\frac{\partial f^{o}(net_{k(r)}^{(L)})}{\partial net_{k(r)}^{(L)}} y_{j(r)}^{(L)} \end{aligned}$$

Weight adjustment for the hidden layer was calculated by:

$$\begin{aligned} v_{ij(r)}^{(L)}(t+1) &= v_{ij(r)}^{(L)}(t) - \eta^{(L)} \frac{\partial E_{(r)}}{\partial v_{ij(r)}^{(L)}(t)} \\ &= v_{ij(r)}^{(L)}(t) - \eta^{(L)} \sum_{k} \left((o_k - d_k)\frac{\partial f^{o}(net_{k(r)}^{(L)})}{\partial net_{k(r)}^{(L)}} w_{jk(r)}^{(L)} \right) \frac{\partial f^{h}(net_{j(r)}^{(L)})}{\partial net_{j(r)}^{(L)}} x_{i(r)}^{(L)} \end{aligned}$$

Backward pass for the global connections was derived similarly. Simulation results are shown in the simulation section.

Results and Discussion

Database

The sampling data set contains trials of motions conducted by 249 subjects. Each trial had twenty sampling data points. Every subject conducted all the trials. Therefore, the total number of data points N is:

$$N = n_{subjects} \times n_{trials} \times 20 = 29880$$

where $n_{subjects}$ is the number of subjects and n_{trials} is the number of trials.

Since the data was derived from previously collected studies at the OSU Biodynamics Laboratory, the subject population was predefined along with the number of subject conducting a given set of conditions. Table I provides a summary of the number of subjects in each of the condition domains.

Table I
Summary of Subjects

Weight Lifted								
3.4 kg	6.8 kg	10.2 kg	11.4 kg	13.6 kg	22.7 kg	27.3 kg		
10	197	10	68	158	49	13		
Task Asymmetry at Origin								
90 ccw	60 ccw	30 ccw	sag sym	30 cw	45 cw	60 cw	90 cw	135 cw
	26	10	226	10	33	88	10	10
Task Asymmetry at Destination								
90 ccw	60 ccw	30 ccw	sag sym	30 cw	45 cw	60 cw	90 cw	135 cw
52	16		184			16		
Height of Lift at Origin								
Floor	Knee	Knuckle	Elbow	Shoulder				
72	184	52	16	16				
Height of Lift at Destination								
Floor	Knee	Knuckle	Elbow	Shoulder				
	16		236	16				
Number of Hand Used During Lift (handedness)								
Two	Lt Hand	Rt Hand						
10	236	20						
Lifting Style								
Stoop	Squat	Free						
23	23	213						

Input variables identification

Not knowing which variables really affect the EMG signals, all the associated kinematic and kinetic variables as well as anthropometric variables were inputted into the model (Tables II and III). The 9 kinematic and 3 kinetic variables are dynamic variables which change their values during the entire motion of each trial. While the fifteen anthropometric variables are static variables that relate to the body measurements of the subjects and they are the same for a particular subject. The objective was to find out how these variables affect the EMG signals. Each data point consist of 27 input variables (x_i, $i=1,2,...,27$) and 10 output variables (y_j, $j=1,2,...,10$). The outputs were EMG signals of 10 trunk muscles (see Table IV).

TABLE II
Kinematic and Kinetic Variables (Dynamic)

Sagittal Trunk Moment	Sagittal Trunk Angle
Sagittal Trunk Velocity	Sagittal Trunk Acceleration
Lateral Trunk Moment	Lateral Trunk Angle
Lateral Trunk Velocity	Lateral Trunk Acceleration
Axis Trunk Moment	Axis Trunk Angle
Axis Trunk Velocity	Axis Trunk Acceleration

TABLE III
Anthropometric Variables (Static)

Age	Upper Leg Length	Trunk Depth (pelvis)
Body Weight	Upper Arm Length	Trunk Breadth (pelvis)
Standing Height	Lower Leg Length	Trunk Depth (xyphoid)
Shoulder Height	Lower Lrm Length	Trunk Breadth (xyphoid)
Elbow Height	Spine Length	Trunk Circumference

TABLE IV
Name of the Ten Trunk Muscles

Right latissimus dorsi	Left latissimus dorsi
Right erector spine	Left erector spine
Right rectus abdominus	Left rectus abdominus
Right external oblique	Left external oblique
Right internal oblique	Left internal oblique

To calculate the x_i-y_j relationships and identify key variables of the system, the distribution of the original data set without clustering was first used. For some of the input-output relationships, there was a drop in the middle of the range of variable x_i. An example is shown in Figure 13 (A). This relationship was incorrect for some variables and was uninterpretable from the ergonomics point of view. Sometimes when different portions of the data set were used, different relationships were obtained. Therefore, the distribution of the sampling data affected the result. Certain conditions may have appeared more frequently during the motion than other conditions and thus have distorted the fuzzy average curve.

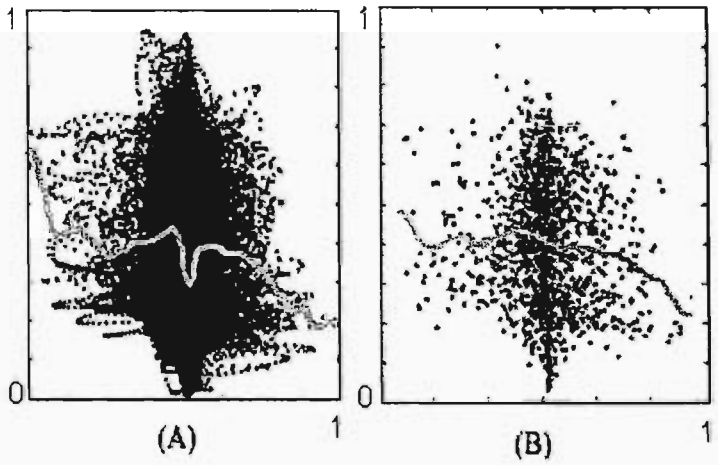

Figure 13: The neural network structure with local connections

Next, FAFCD was used to obtain the input-output relationships on the new data set produced using fuzzy clustering. Procedures in the flowchart as shown in Figure 7 were followed. All input variables in the original data set were normalized to the range of [*0, 1*]. The output variables (the normalized EMG signals) were also in the range of [*0, 1*]. Then the data points were clustered as described earlier. A summary of cluster properties is shown in Table IV. Those clusters contain less than 10 data points (about 0.033% of the total) were considered as outliers and were removed from the data set.

Table IV
Summary About The Clusters

Total number of data points	29880
Number of clusters	4816
Range of number of data points in the clusters	1 - 1456
Number of clusters with less than 10 data points	66

Next in the process, FCM algorithm was used to find centers of the rest clusters. By comparing the Euclidean distance of each data point in a cluster to the center of this cluster, the closest data point to the center was found. Using this data point to represent the corresponding cluster, a new data set with a different distribution to the original data set was obtained. On this new data set, the fuzzy average of y_j in each x_i - y_j space was calculated. Figure 13 (B) shows the result of the same example as in Figure 13 (A), using FAFCD. As expected, the drop in Figure 13 (A) disappeared and the result has a clear physical explanation now. Figure 14 shows the relationship between all kinematic and kinetic variables and EMG signals of muscle Right Latissimus Dorsi. Figure 15 shows the relationship between all subject variables and EMG signals of this muscle. The relationships of inputs to the other muscles were obtained similarly. With these relationships, a better understanding to the muscle activities was obtained. At the same time, the importance of the input variables were indicated by their Influence Rate *R*. Table V shows the Influence Rate of each kinematic and kinetic variable to each output. The first row is name of the muscle; the first column is name of kinematic and kinetic variables. Table VI shows the influence rate of each anthropometric variable to each output. The first row is name of the muscle; the first column is name of the anthropometric variable. Based on the Influence Rate, key variables were identified.

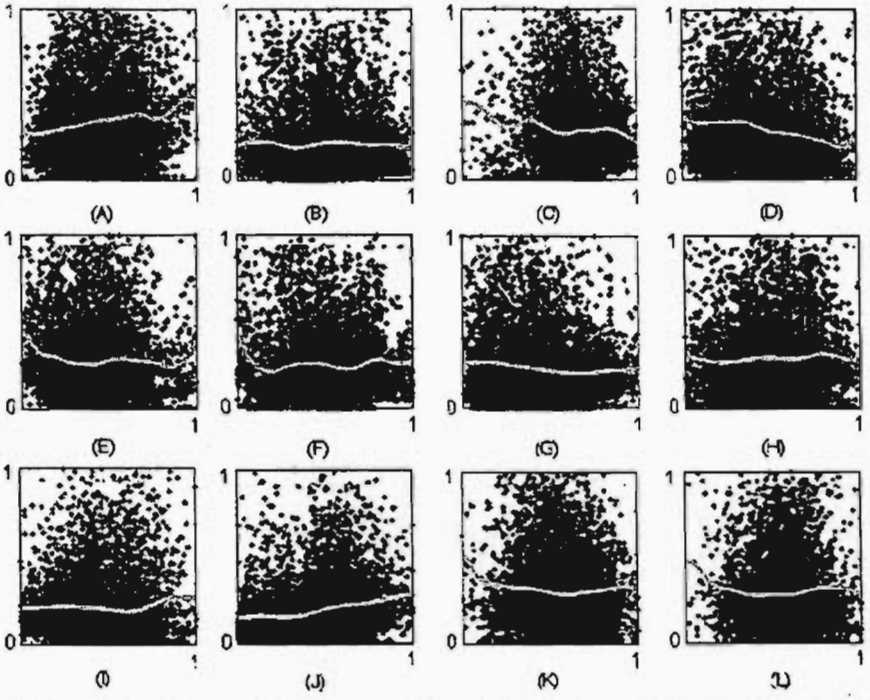

Figure 14: Relationship between the kinematic and kinetic variables (x axis) and EMG signals (y axis) of the muscle Right Latissimus Dorsi (RLD). Variables from (A) to (L) are in the same sequence as in Table V.

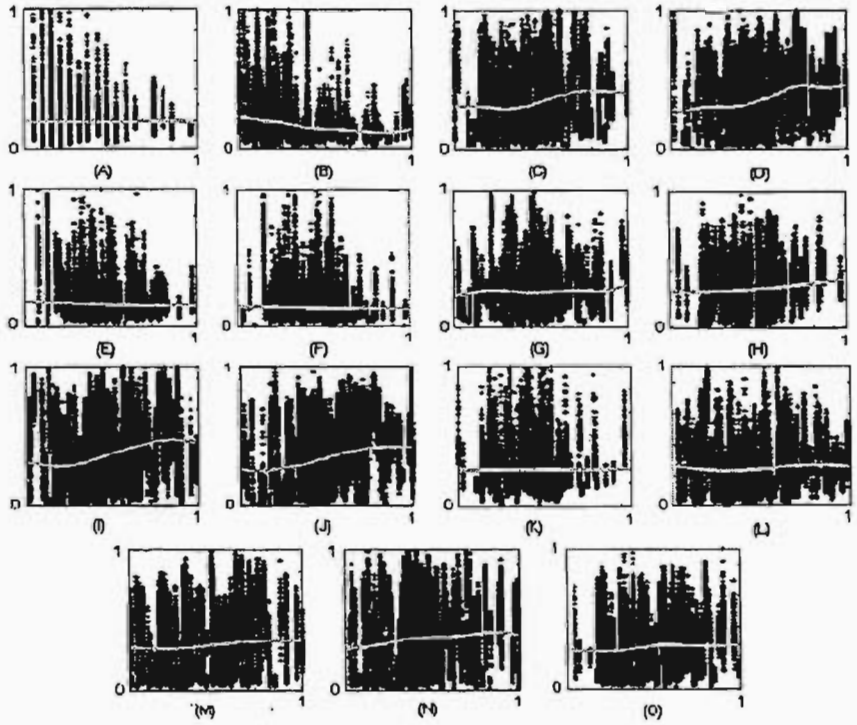

Figure 15: Relationship between the subject variables (x axis) and EMG signals (y axis) of the muscle Right Latissimus Dorsi (RLD). Variables from (A) to (O) are in the same sequence as in Table VI.

According to Tables V and VI, significance of the kinematic variables and anthropometric variables are ranked as shown in Figure 16 and Figure 17, respectively. It is clear that kinematic variables are more significant than subject variables. Thus, these 9 kinematic and 3 kinetic variables should all be selected as inputs in modeling. This is a reasonable conclusion and agrees with our hypothesis. As for subject variables, four variables (standing height, shoulder height, lower arm length, and spine length) are more significant than the others. These variables should also be taken as inputs in modeling. However, by examining the two variables "standing height" and "shoulder height" in Table VI, it was found that the Influence Rates of these two variables are very similar, for every muscle. In other words, these two variables were correlated. They were dependent variables to each other. Therefore, one of them was removed.

TABLE V

Influence Rate of Kinematic and Kinetic Variables

(SAG=Sagittal, LAT=Lateral, MOM=Moment, ANG=Angle, VEL=Velocity, and ACC=Acceleration)

	RLD	LLD	RES	LES	RRA	LRA	REO	LEO	RIO	LIO	Average
Sag. trunk mom.	0.208	0.220	0.182	0.149	0.049	0.087	0.177	0.223	0.260	0.133	0.1688
Lat. trunk mom.	0.046	0.113	0.332	0.293	0.129	0.110	0.054	0.101	0.093	0.207	0.1478
Axis trunk mom.	0.136	0.209	0.169	0.220	0.081	0.089	0.037	0.062	0.015	0.089	0.1107
Sag. trunk ang.	0.116	0.100	0.149	0.121	0.057	0.058	0.073	0.100	0.187	0.143	0.1104
Lat. trunk ang.	0.135	0.094	0.106	0.109	0.042	0.061	0.065	0.047	0.088	0.139	0.0886
Axis trunk ang.	0.124	0.079	0.172	0.310	0.135	0.141	0.066	0.068	0.122	0.165	0.1382
Sag. trunk vel.	0.055	0.069	0.199	0.196	0.031	0.114	0.106	0.090	0.124	0.225	0.1209
Lat. trunk vel.	0.045	0.042	0.172	0.094	0.050	0.162	0.079	0.061	0.131	0.145	0.0981
Axis trunk vel.	0.072	0.074	0.090	0.087	0.050	0.207	0.029	0.090	0.181	0.081	0.0961
Sag. trunk acc.	0.139	0.095	0.118	0.167	0.071	0.046	0.095	0.053	0.142	0.104	0.1030
Lat. trunk acc.	0.160	0.088	0.100	0.079	0.077	0.087	0.028	0.070	0.104	0.077	0.0870
Axis trunk acc.	0.168	0.080	0.179	0.139	0.059	0.078	0.079	0.126	0.116	0.070	0.1094

TABLE VI

Influence Rate of Antropometric Variables (LEN=Length, DEP=Depth, PEL=Pelvis, BR=Breadth, XY=Xyphoid, and CIR=Circumference)

	RLD	LLD	RES	LES	RRA	LRA	REO	LEO	RIO	LIO	Average
Age	0.002	0.001	0.005	0.005	0.004	0.001	0.002	0.002	0.001	0.003	0.0026
Body weight	0.088	0.068	0.071	0.103	0.013	0.026	0.030	0.029	0.015	0.052	0.0493
Standing height	0.118	0.074	0.120	0.158	0.048	0.097	0.045	0.056	0.018	0.087	0.0821
Shoulder height	0.120	0.080	0.118	0.155	0.038	0.099	0.049	0.059	0.021	0.081	0.0820
Elbow height	0.043	0.013	0.031	0.057	0.016	0.016	0.025	0.005	0.022	0.027	0.0255
Upper leg len.	0.032	0.021	0.013	0.003	0.005	0.009	0.013	0.023	0.003	0.008	0.0130
Lower leg len.	0.099	0.060	0.086	0.123	0.036	0.055	0.043	0.036	0.016	0.086	0.0640
Upper arm len.	0.078	0.020	0.030	0.053	0.008	0.025	0.024	0.019	0.006	0.029	0.0292
Lower arm len.	0.090	0.081	0.151	0.164	0.019	0.062	0.039	0.034	0.033	0.112	0.0785
Spine len.	0.082	0.055	0.117	0.125	0.067	0.087	0.035	0.048	0.066	0.077	0.0759
Trunk dep. pel.	0.009	0.007	0.022	0.009	0.007	0.016	0.018	0.012	0.010	0.008	0.0118
Trunk br. pel.	0.055	0.051	0.022	0.030	0.045	0.018	0.033	0.004	0.036	0.008	0.0302
Trunk dep. xy.	0.038	0.044	0.027	0.057	0.040	0.020	0.020	0.017	0.013	0.035	0.0311
Trunk br.xy.	0.080	0.056	0.066	0.093	0.032	0.032	0.018	0.021	0.027	0.063	0.0488
Trunk cir.	0.047	0.040	0.032	0.052	0.014	0.058	0.055	0.027	0.037	0.031	0.0393

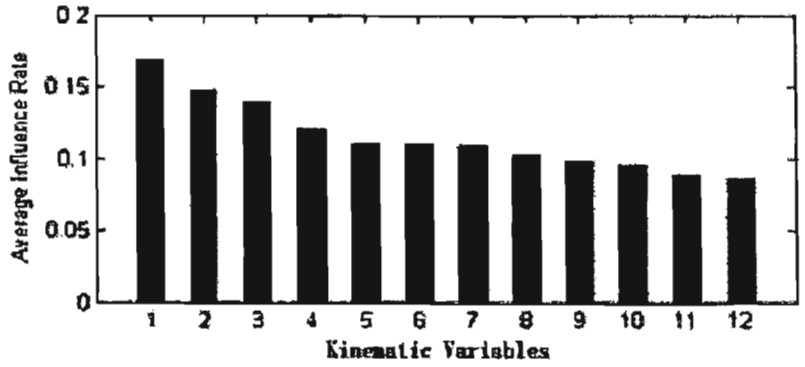

Figure 16: Rank kinematic and kinetic variables by their Average Influence Rate (1: Sagittal trunk moment, 2: Lateral trunk moment 3: Axis trunk angle 4: Sagittal trunk velocity, 5: Axis trunk moment, 6: Sagittal trunk angle, 7: Axis trunk acceleration, 8: Sagittal trunk acceleration, 9: Lateral trunk velocity, 10: Axis trunk velocity, 11: Lateral trunk angle, 12: Lateral trunk acceleration).

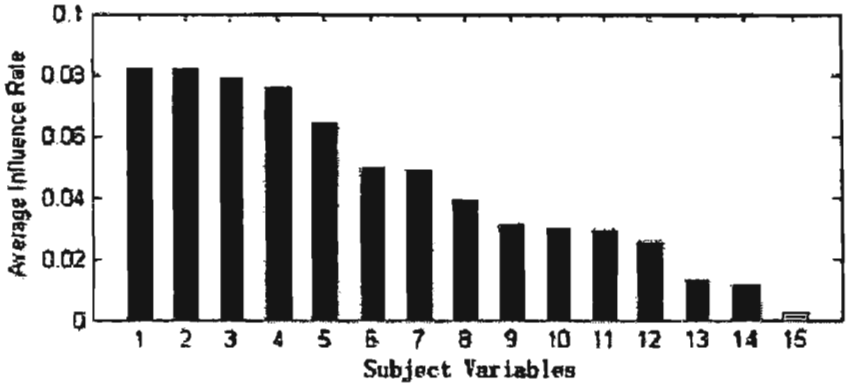

Figure 16: Rank anthropometric variables by their Average Influence Rate (1: Standing height, 2: Shoulder height, 3: Lower arm length, 4:Spine length, 5: Lower leg length, 6: Body weight, 7: Trunk breadth (xyphoid), 8: Trunk circumference, 9: Trunk depth (xyphoid), 10: Trunk breadth (pelvis), 11: Upper arm length, 12: Elbow height, 13: Upper leg length, 14: Trunk depth (pelvis), 15: Age)

Neural network model for EMG estimation

The current EMG estimation model was built based on the laboratory-collected EMG data sets along with related information about the subject and lifting conditions. With the same model structure, different individual models were built for different lifting conditions. It was not feasible to build a "universal" model for all lift conditions because it would have decreased the generalization ability and estimation accuracy of the EMG levels. Different lift

conditions were described by variables such as object weight, lift height, asymmetry, handedness, etc. For model validation, the laboratory measured EMG data were compared with the estimated EMG data obtained from the neural network model. The performance of the current model was tested by comparing the output with the basic models described above.

As stated before, input variables were identified using FAFCD. After pruning, all 6 kinematic, 3 kinetic and 4 subject variables (standing height, lower arm length, spine length, and lower leg length) were kept to serve as input of the model.

Data Preprocessing

Ill-conditioning of the data would have greatly decreased the performance of a neural network model. Thus, the data was pre-processed before they can be used in the neural network model. First, the data for the kinematic trails were synchronized across trials. The synchronization included making sure that the start and end points of the lifted occurred at the relative same time for al trials, which increased the prediction precision. Some subjects moved faster than the others in a lift. Subsequently, the sampling points of their motions were fewer than those move slower. Since the input dimension of the model had to be constant, the data was re-sampled using a specially designed Matlab software program so that all the data had the same number of sampling points.

The raw kinematic and kinetic input data had different ranges which are troublesome to the development of neural network. As a result, the data was normalized to the range from -2.0 to 2.0. Subject variables are also normalized to the range from -2.0 to 2.0 with gender coded as male: 2 and female: -2. Because the unipolar sigmoid activation function was used in the output layer, the target (EMG) need to be normalized to the range of 0.15 to 0.85, to avoid the saturation regions of the activation function.

Model Parameters

Some parameters of the model are listed below (Table VII), in which "global" stands for the global connections in the model, and "local" stands for the local connections in the model. For example, "Global learning rate" means the learning rate of the global connections. "Local learning rate" means the learning rate of the local connections (the global connections and the local connections often need different learning rates, in order to make sure they can be fully trained at the same time). The effect of the number of hidden neurons was empirically investigated.

Table VII

MODEL PARAMETERS

Global hidden units	$30 + 30$
Local hidden units	9
Global learning rate	0.01
Local learning rate	0.05
Momentum	0.8
Maximum Epoch Number	1000

Other considerations

Nguyen-Widrow initialization [81] method was used to initialize the weights. Simulations show that in the current model, this kind of initialization helps the model to avoid saturation of some neurons. It was found that the states of hidden neurons often became saturated (-1 or 1) quickly, after several training epochs. This happens even when the inputs have been normalized and the initial weights are small. The saturation of the hidden neurons makes the output of the network become very reluctant to change. Nguyen-Widrow initialization has been found to solve this problem very well.

Cross-validation was used to prevent the network from over-fitting the patterns. The subjects are divided into a training set, a test set and a validation set. Every so often, the network performance is checked on the validation set. If the rise of error on the validation set reaches the limit, the learning is stopped.

Model Performance

Since the current model has more parameters than the basic model, its training time was longer than that of the basic model. However, the test time of the current model was shorter than that of the basic model which results from the one sampling point at one time method for the previous model as compared to all sampling points at once for the current method.

The mean absolute errors (MAEs) between the actual and model-estimated normalized EMG values were calculated. To evaluate how good the model-estimated EMG signals fit the actual EMG signals, R-Square was also calculated. R-square measured how successful the fit was in explaining the variation of the data. Figure 18 shows EMG signal of muscle "Left Erector Spine" in a motion. The solid curves are the predicted EMG signals. It can be seen that for the model without local connections, although the MAE of the prediction was not bad, the prediction doesn't fit the curve very well in the small regions. By extracting the local features and modifying the output locally, the model with local connections produced a better prediction.

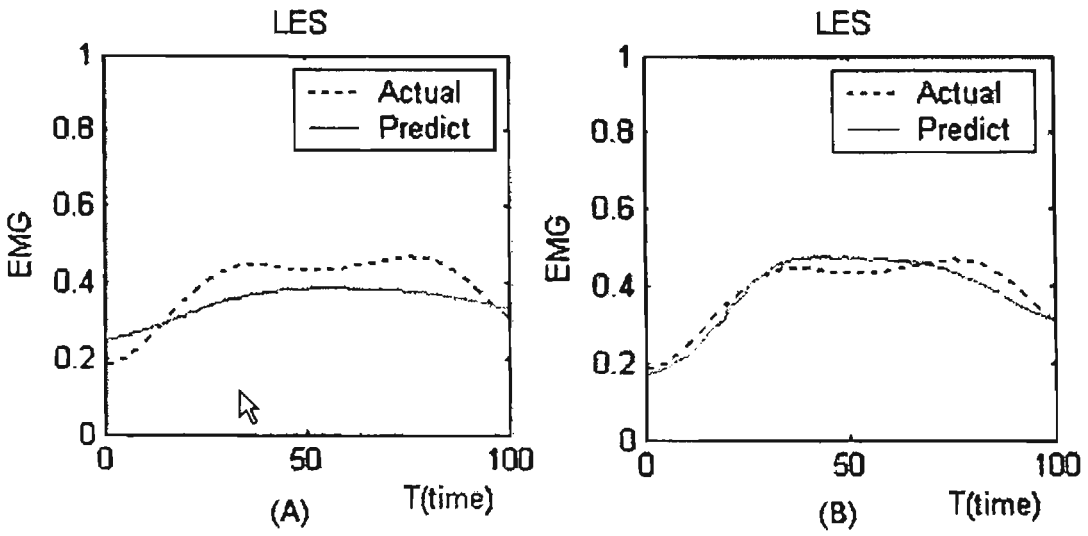

Figure 18: Local connections improve locality. (A) Without local connections. (B) With local connections.

As mentioned before, the network without local connections suffers from incorrect timing. This is demonstrated in Figure 19 (A). The dotted line is the actual EMG signal of muscle "Left Erector Spine". The rear part of the motion was missing, resulting in the recorded data start at the right time but ending before the motion finished.

For some of the trials, not all of the entire motion was recorded or the type of lift for some subjects only had a portion of the traditional motion. While the normal motion required EMG pattern that follows the trend of first going up, peaking and plateauing, then going down, ending with a low level of EMG. However, some of the trials never have the declining portion at the end of the lift. In Figure 19 (A) the incomplete motion does not follow such trend. But when trying to predict this motion, the neural network will take it as complete. The predicted curve (solid curve) goes down as if the motion is complete. This makes the prediction relatively unsatisfactory. After the local connections are added, the timing is no longer a problem. Since these connections are connected "locally", local features of each sampling point are extracted by them. Figure 19 (B) shows the improved prediction.

Statistical Summary

Generally, the developed model is capable of estimating normalized EMG values with satisfactory results. The total number of trials evaluated is 13440. For all muscles, the overall average MAE is 7.56%; the overall average R-square is 0.5437 (Tables VIII and IX). Average MAE and average R-square for different muscles are listed in the following tables. It was shown that four muscles (Right Rectus Abdominus, Left Rectus Abdominus, Right External Oblique, and Left External Oblique) have smaller MAEs than others which resulted from the EMG signals of these four muscles are more or less static during the lifting motions (antagonistic muscles). Therefore, they are easier to predict than others.

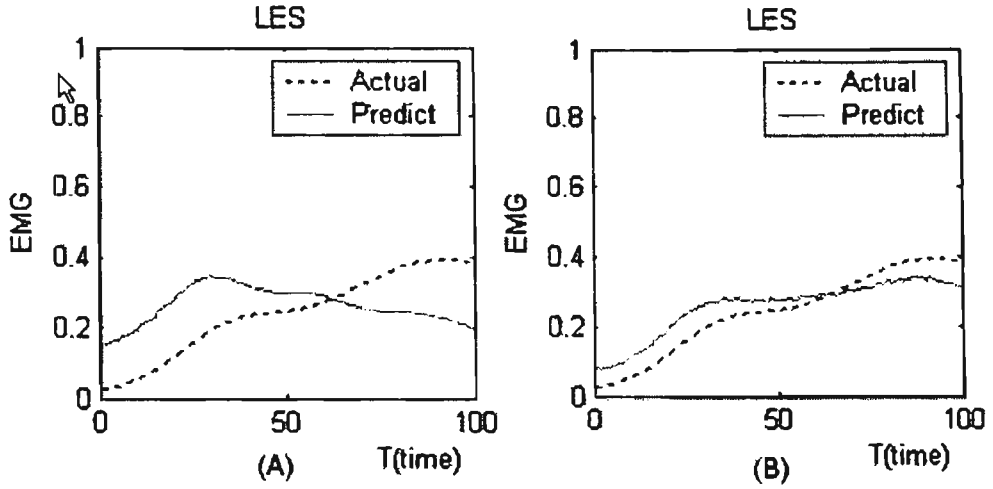

Figure 19: Local connections don't suffer from incorrect timing. (A) Without local connections. (B) With local connections.

Table VIII

Average Mean Absolute Errors (MAE) for all muscles when comparing predicted to measured EMG

Muscles	MAE	Standard Deviation
RLD	7.22%	5.26%
LLD	7.26%	5.22%
RES	12.04%	7.55%
LES	12.50%	7.81%
RRA	3.71%	3.06%
LRA	3.64%	3.49%
REO	4.31%	3.04%
LEO	4.73%	3.58%
RIO	9.64%	6.33%
LIO	10.50%	6.54%

Table IX

Average R-Squared for all muscles when comparing predicted to measured EMG

Muscles	R-square	Standard Deviation
RLD	0.507	0.3086
LLD	0.507	0.3008
RES	0.688	0.2755
LES	0.709	0.2667
RRA	0.341	0.2786
LRA	0.341	0.2782
REO	0.492	0.3092
LEO	0.547	0.3065
RIO	0.629	0.2885
LIO	0.676	0.2802

Statistical Results for Different Task Conditions

The following tables provides of summary statistics for the individual conditions followed by figures for overall workplace characteristics.

Table X: **Sagittally symmetric lift from floor to waist of 6.8 kg box**

# of Files	Object Weight	Origin Asymmetry	Destination Asymmetry	Origin Height	Destination Height
374	about 6.8 kg	Sagittal	Sagittal	about 0 cm	about 100 cm

Muscles	MAE	Standard Deviation	R-square	Standard Deviation
RLD	6.25%	4.32%	0.5954	0.3158
LLD	5.51%	3.47%	0.5864	0.2969
RES	13.95%	8.97%	0.6311	0.3263
LES	13.72%	7.83%	0.6019	0.3283
RRA	3.80%	2.79%	0.2392	0.2404
LRA	4.28%	4.77%	0.3049	0.2697
REO	3.87%	2.53%	0.2791	0.2525
LEO	3.43%	2.61%	0.2856	0.2517
RIO	10.64%	7.70%	0.6167	0.3066
LIO	10.64%	7.39%	0.6213	0.3125

Table XI: Sagittally symmetric lift from floor to waist of 13.6 kg box

# of files	Object Weight	Origin Asymmetry	Destination Asymmetry	Origin Height	Destination Height
373	about 13.6 kg	Sagittal	Sagittal	about 0 cm	about 100 cm

Muscles	MAE	Standard Deviation	R-square	Standard Deviation
RLD	10.23%	6.89%	0.5457	0.2852
LLD	9.08%	5.64%	0.6046	0.2767
RES	16.69%	10.71%	0.6165	0.3376
LES	16.91%	8.65%	0.6093	0.3449
RRA	3.97%	2.80%	0.2469	0.2337
LRA	5.54%	6.62%	0.2687	0.2430
REO	4.54%	3.46%	0.2775	0.2482
LEO	4.51%	3.54%	0.3167	0.2575
RIO	13.47%	8.49%	0.5891	0.3235
LIO	13.10%	8.57%	0.6133	0.3210

Table XII: Sagittally symmetric lift from knee height to waist of 3.4 and 6.8 kg boxes

# of Files	Object Weight	Origin Asymmetry	Destination Asymmetry	Origin Height	Destination Height
744	between 3.4 kg and 6.8 kg	Sagittal	Sagittal	about 50 cm	about 100 cm

Muscles	MAE	Standard Deviation	R-square	Standard Deviation
RLD	4.80%	3.91%	0.4608	0.3238
LLD	4.59%	3.63%	0.4194	0.3202
RES	12.82%	8.80%	0.5891	0.3175
LES	12.71%	8.10%	0.6259	0.2876
RRA	3.39%	2.82%	0.2929	0.2536
LRA	3.42%	2.99%	0.3247	0.2748
REO	2.86%	1.97%	0.4346	0.3024
LEO	2.88%	2.15%	0.4613	0.3068
RIO	9.53%	6.83%	0.5712	0.3027
LIO	9.56%	6.70%	0.6046	0.2957

Table XIII: Sagittally symmetric lift from knee height to waist of 10.2 to 13.6 kg boxes

# of files	Object Weight	Origin Asymmetry	Destination Asymmetry	Origin Height	Destination Height
1507	Between 10.2 kg and 13.6 kg	Sagittal	Sagittal	about 50 cm	about 100 cm

Muscles	MAE	Standard Deviation	R-square	Standard Deviation
RLD	6.57%	5.45%	0.4700	0.3096
LLD	6.40%	4.93%	0.4459	0.3093
RES	13.14%	8.19%	0.6909	0.2921
LES	12.63%	7.83%	0.6837	0.2918
RRA	3.89%	3.79%	0.4636	0.3145
LRA	3.51%	3.80%	0.4829	0.3053
REO	3.16%	2.27%	0.5638	0.3277
LEO	3.30%	2.61%	0.5499	0.3259
RIO	9.89%	6.92%	0.6228	0.3078
LIO	10.27%	6.64%	0.6271	0.3105

Table XIV: Sagittally symmetric lift from knee height to waist of 22.7 kg to 27.3 kg boxes

# of files	Object Weight	Origin Asymmetry	Destination Asymmetry	Origin Height	Destination Height
468	Between 22.7 kg and 27.3 kg	Sagittal	Sagittal	about 50 cm	about 100 cm

Muscles	MAE	Standard Deviation	R-square	Standard Deviation
RLD	7.76%	4.31%	0.5444	0.3103
LLD	8.05%	6.39%	0.5467	0.2948
RES	12.35%	6.98%	0.8135	0.2281
LES	14.42%	9.51%	0.7981	0.2462
RRA	3.91%	3.52%	0.4225	0.3016
LRA	2.86%	2.49%	0.4789	0.3043
REO	3.33%	2.25%	0.4479	0.2897
LEO	3.83%	3.31%	0.4906	0.2901
RIO	13.38%	7.80%	0.7730	0.2565
LIO	10.31%	5.54%	0.7719	0.2344

Table XV: Asymmetric lift from knee height to waist of 22.7 kg to 27.3 kg boxes

# of files	Object Weight	Origin Asymmetry	Destination Asymmetry	Origin Height	Destination Height
442	Between 22.7 kg and 27.3 kg	about 60 Clockwise	Sagittal	About 50 cm	about 100 cm

Muscles	MAE	Standard Deviation	R-square	Standard Deviation
RLD	7.71%	4.94%	0.4864	0.2995
LLD	9.51%	5.05%	0.5732	0.2950
RES	11.42%	6.93%	0.7358	0.2598
LES	15.77%	9.41%	0.8098	0.2149
RRA	3.96 %	3.41%	0.3421	0.2708
LRA	2.89 %	2.61%	0.3965	0.2912
REO	3.94 %	2.72%	0.3979	0.2835
LEO	7.22 %	5.34%	0.6349	0.2865
RIO	10.09 %	6.08%	0.6340	0.2743
LIO	13.62%	7.08%	0.7792	0.2606

Table XVI: Asymmetric lift from knee height to waist of 13.6 kg boxes

# of files	Object Weight	Origin Asymmetry	Destination Asymmetry	Origin Height	Destination Height
271	about 13.6 kg	Between 30 Counter-Clockwise to 60 Counter-Clockwise	Sagittal	about 50 cm	about 100 cm

Muscles	MAE	Standard Deviation	R-square	Standard Deviation
RLD	11.65%	8.24%	0.6495	0.2754
LLD	7.34%	5.77%	0.5089	0.3066
RES	11.24%	6.99%	0.8717	0.1567
LES	9.68%	6.50%	0.8646	0.1542
RRA	3.03%	2.46%	0.4130	0.2920
LRA	4.84%	4.72%	0.4817	0.3000
REO	4.33%	3.05%	0.5641	0.3177
LEO	3.11%	2.12%	0.4563	0.3141
RIO	10.86%	6.72%	0.8379	0.1876
LIO	7.79%	5.82%	0.7380	0.2543

Table XVII: Asymmetric lift from floor to waist of 6.8 kg boxes

# of files	Object Weight	Origin Asymmetry	Destination Asymmetry	Origin Height	Destination Height
375	About 6.8 kg	Between 45 clockwise to 60 Clockwise	Sagittal	about 0 cm	about 100 cm

Muscles	MAE	Standard Deviation	R-square	Standard Deviation
RLD	6.59%	4.36%	0.5893	0.3052
LLD	6.18%	3.86%	0.5902	0.2883
RES	13.64%	9.77%	0.6180	0.3217
LES	14.63%	8.95%	0.6102	0.3275
RRA	4.52%	3.96%	0.2603	0.2558
LRA	4.64%	5.18%	0.3289	0.2768
REO	4.15%	2.75%	0.2958	0.2683
LEO	4.27%	2.88%	0.4977	0.3163
RIO	10.51%	7.68%	0.5203	0.3198
LIO	11.42%	7.23%	0.6411	0.3211

Table XVIII: Asymmetric lift from floor to waist of 13.6 kg to 22.7 kg boxes

# of files	Object Weight	Origin Asymmetry	Destination Asymmetry	Origin Height	Destination Height
507	Between 13.6 and 22.7 kg	Between 45 clockwise to 60 clockwise	Sagittal	about 0 cm	about 100 cm

Muscles	MAE	Standard Deviation	R-square	Standard Deviation
RLD	10.10%	6.52%	0.5636	0.2807
LLD	11.03%	6.21%	0.6088	0.2670
RES	13.51%	8.08%	0.6743	0.3338
LES	15.72%	7.90%	0.7282	0.2939
RRA	4.81%	4.04%	0.2987	0.2681
LRA	5.03%	3.77%	0.2926	0.2700
REO	5.43%	4.13%	0.3653	0.2889
LEO	6.477%	4.38%	0.4975	0.2975
RIO	12.38%	6.85%	0.5607	0.3180
LIO	13.50%	7.52%	0.6683	0.3021

Table XIX: Asymmetric lift from knee height to waist of 3.4 kg to 6.8 kg boxes

# of files	Object Weight	Origin Asymmetry	Destination Asymmetry	Origin Height	Destination Height
497	Between 3.4 and 6.8 kg	Between 45 clockwise to 60 Clockwise	Sagittal	about 50 cm	about 100 cm

Muscles	MAE	Standard Deviation	R-square	Standard Deviation
RLD	5.30%	3.59%	0.5538	0.3083
LLD	6.03%	4.69%	0.5994	0.3085
RES	11.20%	7.76%	0.5690	0.3236
LES	13.20%	8.10%	0.7060	0.2655
RRA	3.22%	2.47%	0.3247	0.2566
LRA	3.33%	4.29%	0.3176	0.2668
REO	2.95%	2.13%	0.3353	0.2659
LEO	3.52%	2.61%	0.4636	0.3103
RIO	8.86%	6.11%	0.5732	0.3014
LIO	10.28%	7.04%	0.7089	0.2620

Table XX: Asymmetric lift from knee height to waist of 10.2 kg to 13.6 kg boxes

# of files	Object Weight	Origin Asymmetry	Destination Asymmetry	Origin Height	Destination Height
1039	Between 10.2 kg and 13.6 kg	Between 30 clockwise to 60 clockwise	Sagittal	about 50 cm	about 100 cm

Muscles	MAE	Standard Deviation	R-square	Standard Deviation
RLD	7.34%	5.45%	0.4895	0.3175
LLD	8.09%	5.88%	0.5843	0.2909
RES	10.07%	6.55%	0.6943	0.2895
LES	12.78%	7.98%	0.7503	0.2812
RRA	3.55%	3.24%	0.4388	0.3115
LRA	3.35%	3.69%	0.3713	0.2869
REO	3.01%	2.13%	0.4010	0.2924
LEO	5.24%	3.84%	0.5706	0.3114
RIO	8.09%	6.56%	0.5718	0.3052
LIO	11.23%	7.39%	0.7401	0.2771

Table XXI: Asymmetric lift from knee height to waist of 3.4 kg to 10.2 kg boxes

# of files	Object Weight	Origin Asymmetry	Destination Asymmetry	Origin Height	Destination Height
336	Between 3.4 kg and 10.2 kg	between 90 clockwise and 135 clockwise	Sagittal	about 50 cm	about 100 cm

Muscles	MAE	Standard Deviation	R-square	Standard Deviation
RLD	4.89%	2.92%	0.6119	0.3288
LLD	7.40%	5.02%	0.5304	0.3050
RES	9.31%	4.84%	0.5487	0.3028
LES	10.33%	7.94%	0.7899	0.2344
RRA	2.34%	1.70%	0.4095	0.2835
LRA	2.41%	1.60%	0.3716	0.2839
REO	3.26%	1.92%	0.4346	0.3088
LEO	5.56%	4.52%	0.6973	0.2862
RIO	7.29%	5.69%	0.6089	0.2884
LIO	9.90%	6.93%	0.7770	0.2422

Table XXII: Asymmetric lift from above knee height to waist of 6.8 kg boxes

# of files	Object Weight	Origin Asymmetry	Destination Asymmetry	Origin Height	Destination Height
1630	about 6.8 kg	Sagittal	about 90 Clockwise	about 80 cm	about 105 cm

Muscles	MAE	Standard Deviation	R-square	Standard Deviation
RLD	6.01%	4.39%	0.4061	0.2906
LLD	7.46 %	4.78%	0.5575	0.2898
RES	9.97%	6.04%	0.7155	0.2306
LES	11.19%	6.99%	0.6578	0.2556
RRA	3.35%	2.30%	0.2316	0.2196
LRA	3.57%	2.86%	0.3281	0.2598
REO	3.86%	2.39%	0.4289	0.2873
LEO	5.36%	3.61%	0.6988	0.2418
RIO	7.46%	4.15%	0.6619	0.2729
LIO	10.35%	5.80%	0.6096	0.2698

Table XXIII: Asymmetric lift from above knee height to waist of 11.4 kg boxes

# of files	Object Weight	Origin Asymmetry	Destination Asymmetry	Origin Height	Destination Height
1610	about 11.4 kg	Sagittal	about 90 clockwise	about 80 cm	about 105 cm

Muscles	MAE	Standard Deviation	R-square	Standard Deviation
RLD	7.36%	4.70%	0.3941	0.2937
LLD	8.61%	5.37%	0.5671	0.2852
RES	11.80%	6.33%	0.7064	0.2444
LES	12.82%	7.01%	0.6471	0.2609
RRA	3.84%	2.61%	0.2737	0.2390
LRA	3.66%	3.04%	0.3742	0.2713
REO	4.62%	2.81%	0.4392	0.2781
LEO	6.54%	4.24%	0.7046	0.2391
RIO	9.37%	5.28%	0.6444	0.2828
LIO	12.53%	7.10%	0.6187	0.2699

Table XXIV: Asymmetric lift from above knee height to waist of 6.8 kg boxes

# of files	Object Weight	Origin Asymmetry	Destination Asymmetry	Origin Height	Destination Height
1648	about 6.8 kg	Sagittal	about 90 counter-clockwise	About 80 cm	about 105 cm

Muscles	MAE	Standard Deviation	R-square	Standard Deviation
RLD	7.53%	5.31%	0.5791	0.2832
LLD	6.23%	4.90%	0.4175	0.2780
RES	11.22%	6.51%	0.6983	0.2467
LES	10.51%	6.55%	0.7673	0.2156
RRA	3.65%	3.20%	0.3446	0.2621
LRA	3.58%	2.92%	0.2202	0.2131
REO	5.29%	3.05%	0.6765	0.2546
LEO	3.99%	2.50%	0.4570	0.2926
RIO	9.06%	5.36%	0.6261	0.2656
LIO	8.34%	4.59%	0.7228	0.2525

Table XXV: Asymmetric lift from above knee height to waist of 11.4 kg boxes

# of files	Object Weight	Origin Asymmetry	Destination Asymmetry	Origin Height	Destination Height
1619	about 11.4 kg	Sagittal	about 90 Counter-Clockwise	about 80 cm	About 105cm

Muscles	MAE	Standard Deviation	R-square	Standard Deviation
RLD	8.53%	5.18%	0.5901	0.2869
LLD	7.00%	4.80%	0.3976	0.2739
RES	14.26%	8.06%	0.6939	0.2406
LES	12.39%	7.75%	0.7645	0.2011
RRA	4.01%	2.90%	0.3899	0.2723
LRA	3.55%	2.82%	0.2645	0.2325
REO	6.72%	3.79%	0.6702	0.2523
LEO	4.99%	3.14%	0.4733	0.2788
RIO	11.13%	6.08%	0.6383	0.2519
LIO	9.78%	5.07%	0.7330	0.2387

Statistical Summary as a Function of Workplace Factors

The following figures show the mean absolute error (MAE) and standard deviation (SRD) for each workplace factor categories.

Figure 20: Function of Muscle Activity:

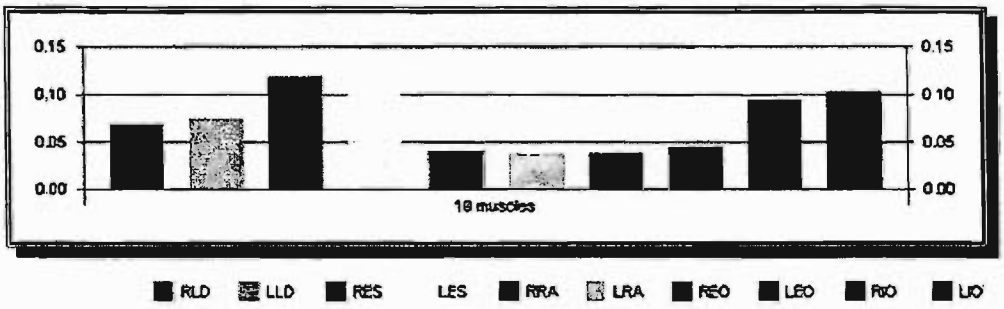

Vertical Axis: mean of MAEs; Horizontal Axis: 10 muscles.

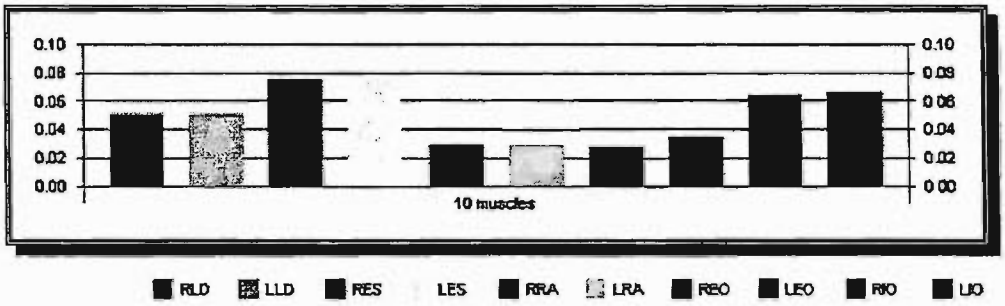

Vertical Axis: STD of MAEs; Horizontal Axis: 10 muscles

Figure 21: Function of Gender

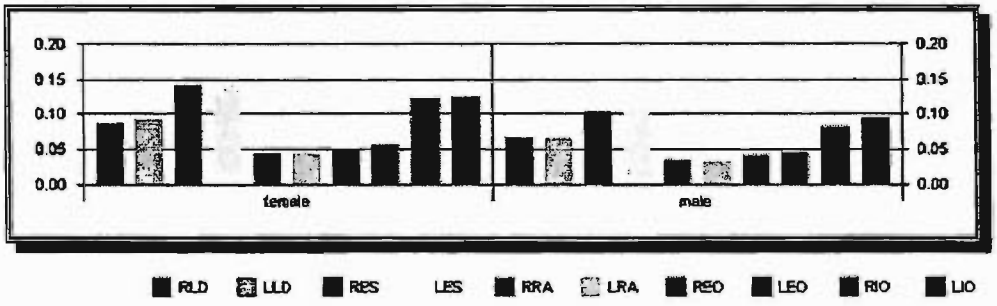

Vertical Axis: mean of MAEs; Horizontal Axis: Gender.

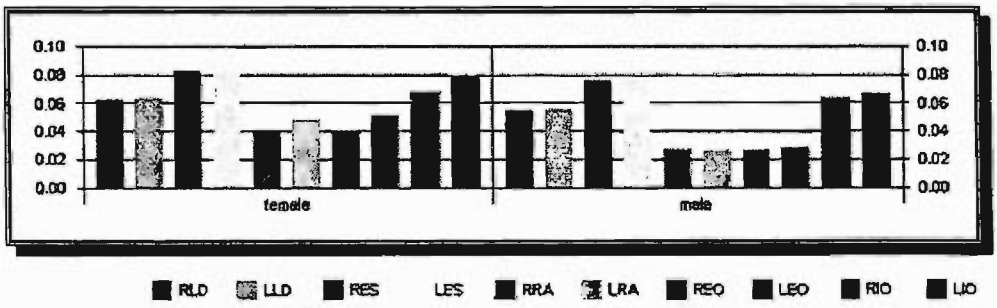

Vertical Axis: STD of MAEs; Horizontal Axis: Gender.

Figure 22: Function of weight of object

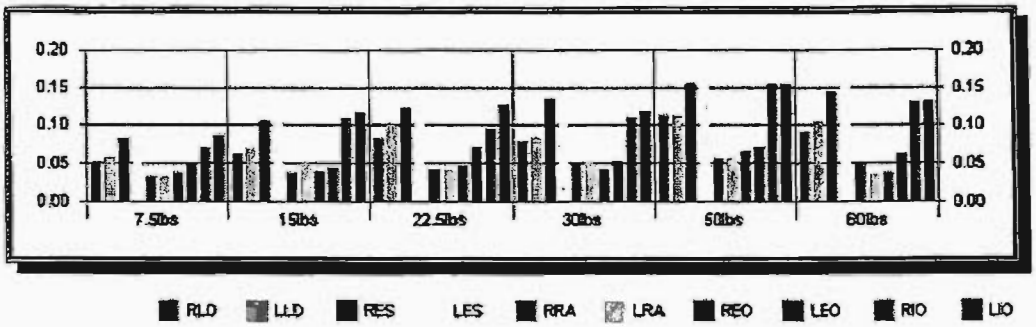

Vertical Axis: mean of MAEs; Horizontal Axis: Weight of Object.

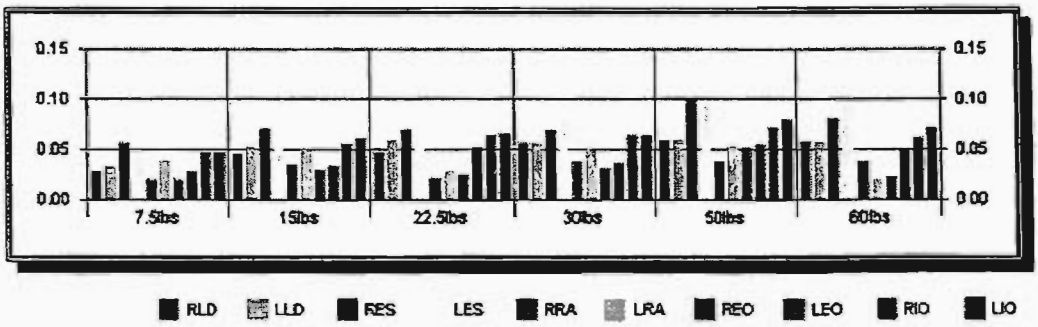

Vertical Axis: STD of MAEs; Horizontal Axis: Weight of Object.

Figure 23: Function of the number of hands

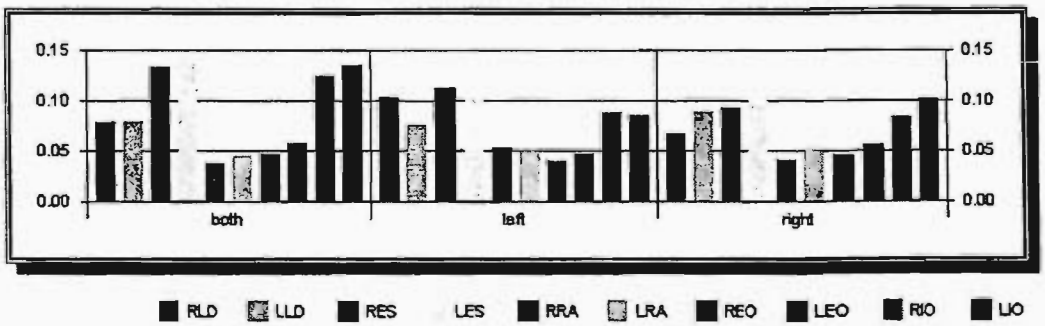

Vertical Axis: mean of MAEs; Horizontal Axis: Handedness.

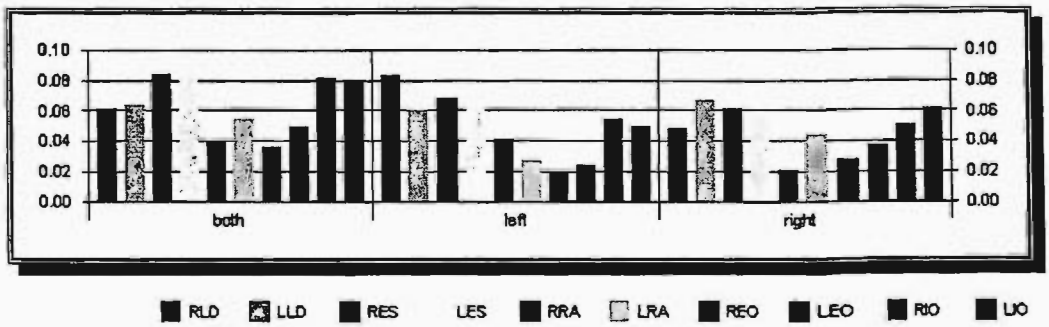

Vertical Axis: STD of MAEs; Horizontal Axis: Handedness.

Figure 24: Function of lifting frequency

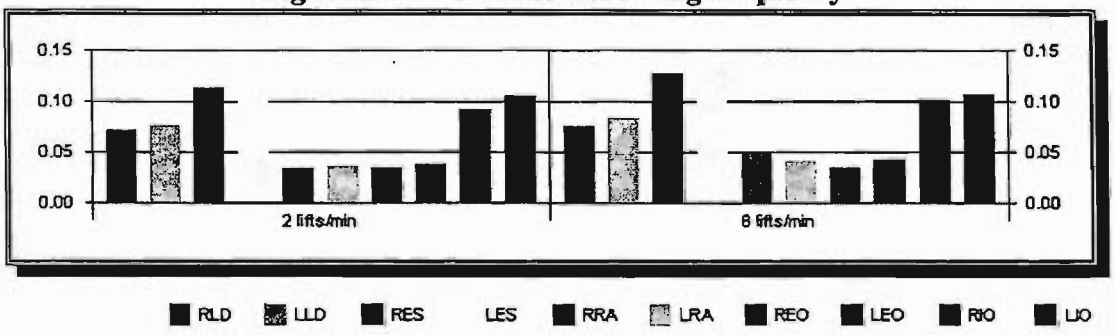

Vertical Axis: mean of MAEs; Horizontal Axis: Frequency.

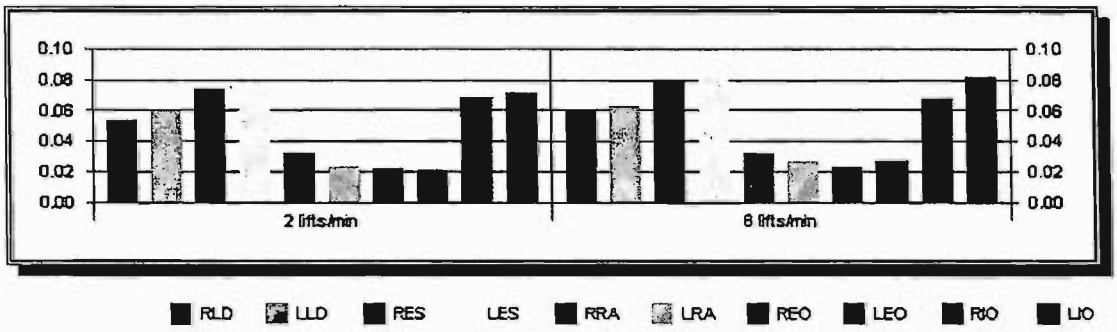

Vertical Axis: STD of MAEs; Horizontal Axis: Frequency.

Figure 25: Function of task asymmetry

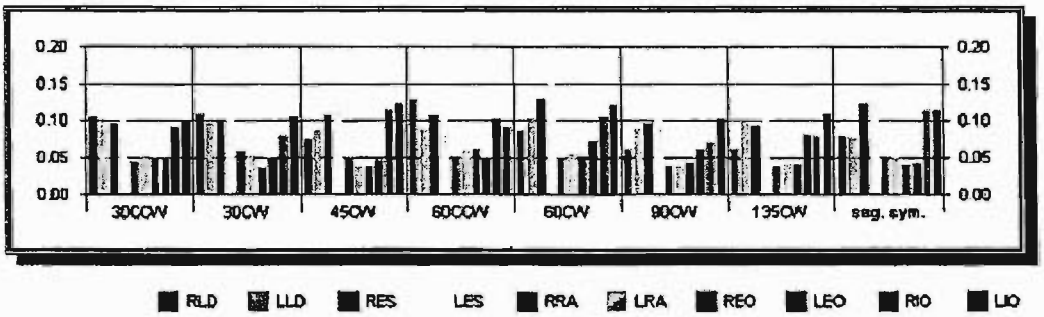

Vertical Axis: mean of MAEs; Horizontal Axis: Asymmetry.

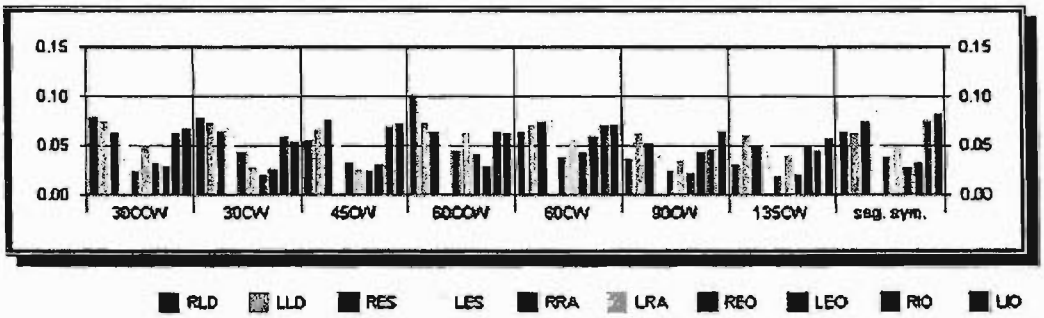

Vertical Axis: STD of MAEs; Horizontal Axis: Asymmetry

Figure 26: Function of lifting style

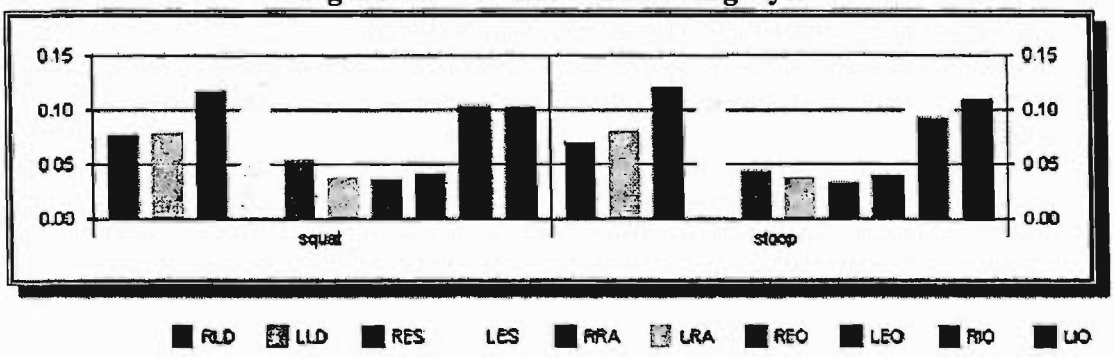

Vertical Axis: mean of MAEs; Horizontal Axis: Style.

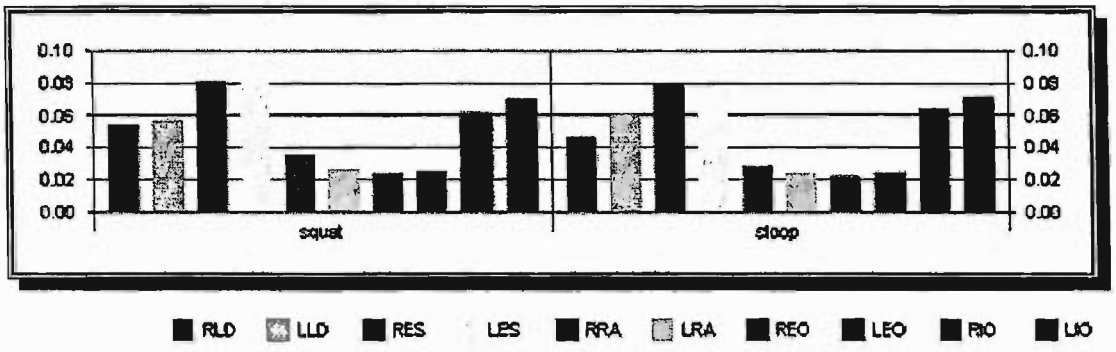

Vertical Axis: STD of MAEs; Horizontal Axis: Style.

Web-Based Software

After the completion of the HYNFE, a software program was developed and integrated into the website (http://osuergo.eng.ohio-state.edu/). The website is an interactive site that allows the user to do one of two things: 1) input kinematic, kinetic, and anthropometric data to acquire predicted muscle activity for the ten trunk muscles, and 2) input muscle activity and kinematic, kinetic and anthropometric variables to further train the HYNFE (only done by the trained user through a separate website with login). The first option will allow the user to obtain muscle activities based on the appropriate input data that is necessary to run the HYNFE. The screen (see Figure 27) has entry boxes for all the appropriate workplace and anthropometric factors to be entered into the software. In addition, the user can upload the file by browsing existing files and selecting the appropriate file. In addition, there is a help screen (Figure 28) that provides further information about the format of the files, the necessary input data, and how to use the software.

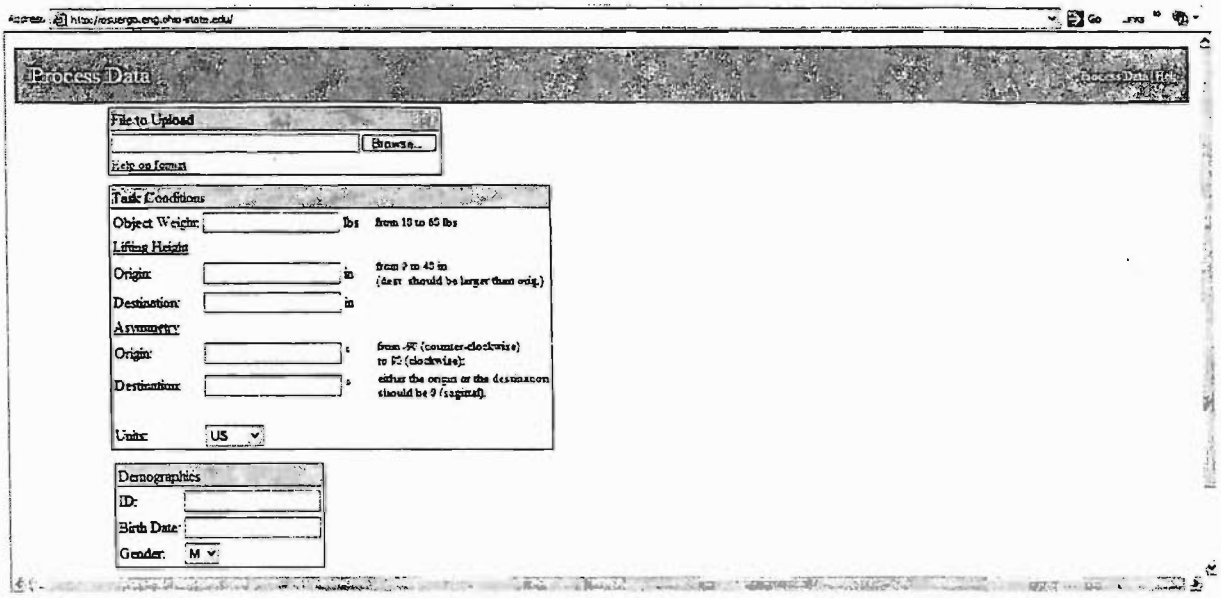

Figure 27: Screen caption of the web program where users can upload kinematic, kinetic, and anthropometric data and obtain predicted muscle activities.

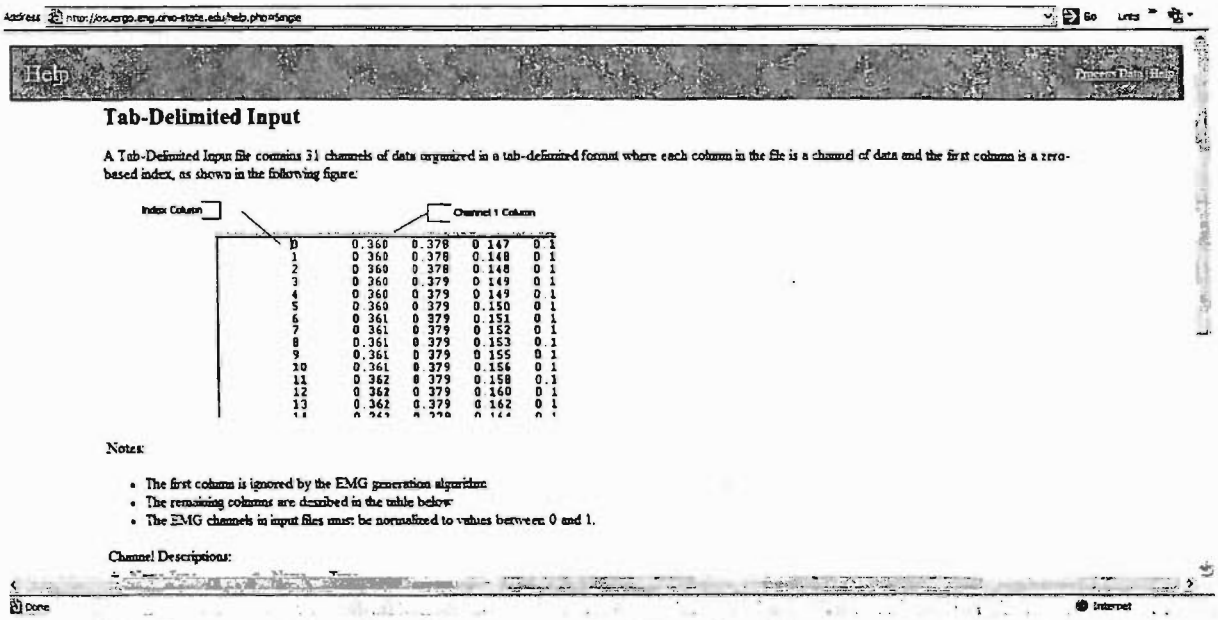

Figure 28: Screen caption of the help screen that describes the necessary information for the program

Loading Comparison of Predicted to Measured EMG

Sixty trials were selected to test the impact of the predicted EMG on the spine loads predicted from the EMG-assisted model. The ultimate goal of any estimate of muscle activity is to estimate the loading on the spine. As such, the validity of the muscle activity prediction was assessed by importing both the actual recorded and predicted data separately into the spine loading model. For both types of muscle activity, the actual kinematic and kinetic data necessary to process the EMG-assisted predictions was utilized. Thus, the only input that changed for a given lift trial was the EMG values.

The results were impressive with regard to how the predicted EMG impacted the model outputs as well as the magnitudes of the spine loads. First, there are three output variables that provide an assessment of the model fidelity: muscle gain—needs to be in a feasible range of 30 N/cm^2 to 120 N/cm^2, r-square (RSQ) between predicted and actual trunk moment—degree of agreement between two trend lines with values above 0.8 being optimal, and average absolute error (AAE)—the average difference between the predicted and measured trunk moments over time with best numbers below 20 Nm. RSQ values are better as they approach 1 while AAE values are better as they approach 0. Based on the benchmarks, the summary of the actual and predicted EMG assessments indicate the predicted EMG modeling was slightly better (Table XXVI). The predicted EMG produced better RSQ values and lower AAE which indicates a better model prediction of the spine loads.

Table XXVI: Summary of model fidelity outcomes when actual and predicted EMG was utilized in the EMG-assisted model

EMG Measure	Gain	R-Square	Average Absolute Error
Predicted	71.0 (29.5)	0.77 (0.16)	17.1 (8.8)
Measured	79.1 (46.0)	0.84 (0.12)	13.1 (7.7)

Second, the magnitudes of the compression, lateral shear, and anterior-posterior shear loads were almost identical between the actual and predicted EMG values. The compression forces were within 0.88% (a difference of 32 N) while shear forces are within 11% of each other (a difference of 14 N for lateral shear and 20 N for A-P Shear). The magnitude of the difference would be virtually biomechanically insignificant. Table XXVII provides a summary of the three-dimensional spine loads for the actual and predicted EMG values. Figures 29 and 30 provide an example of the entire lifting trial.

Table XXVII: Summary of spine load outcomes when actual and predicted EMG was utilized in the EMG-assisted model

EMG Measure	Compression	Anterior-Posterior (A-P) Shear	Lateral Shear
Predicted	3633.0 (934.1)	898.8 (481.3)	139.4 (101.3)
Measured	3665.1 (1043.7)	878.7 (455.8)	125.2 (88.5)
Percent Difference	0.88%	2.24%	10.19%

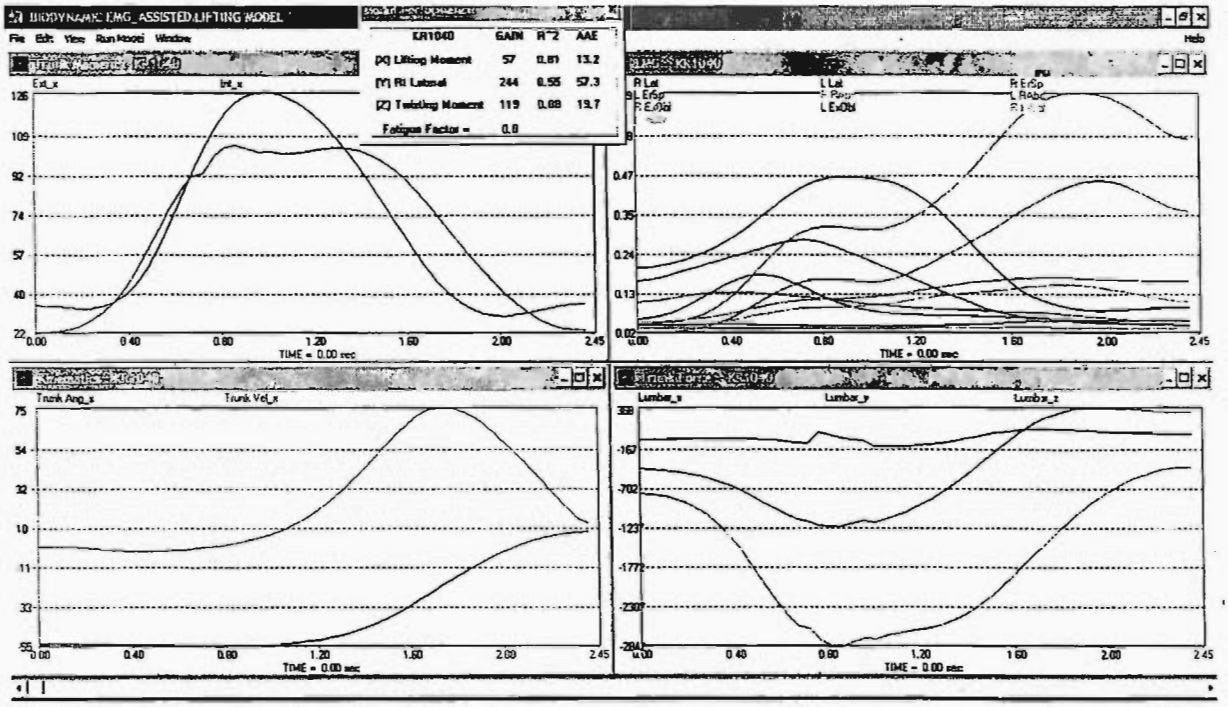

a. Actual EMG Utilized to Predict Spine Loads

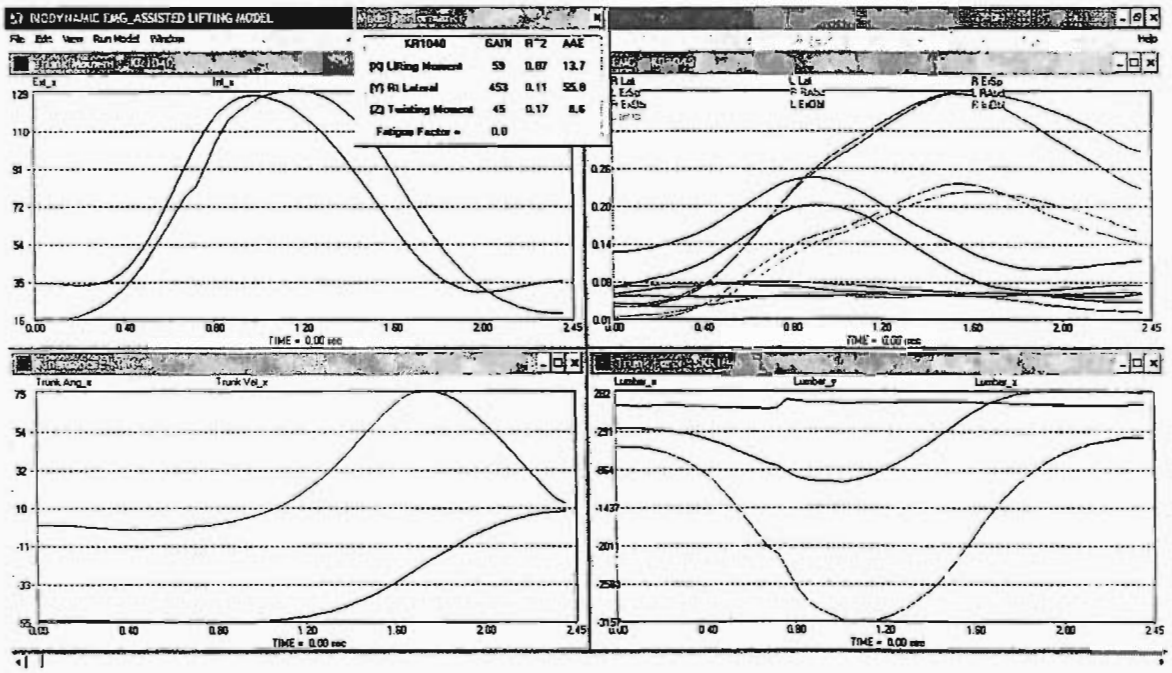

b. Predicted EMG Utilized to Predict Spine Loads

Figure 29: First example of spine loads based on the actual and predicted EMG as predicted by the EMG-assisted model.

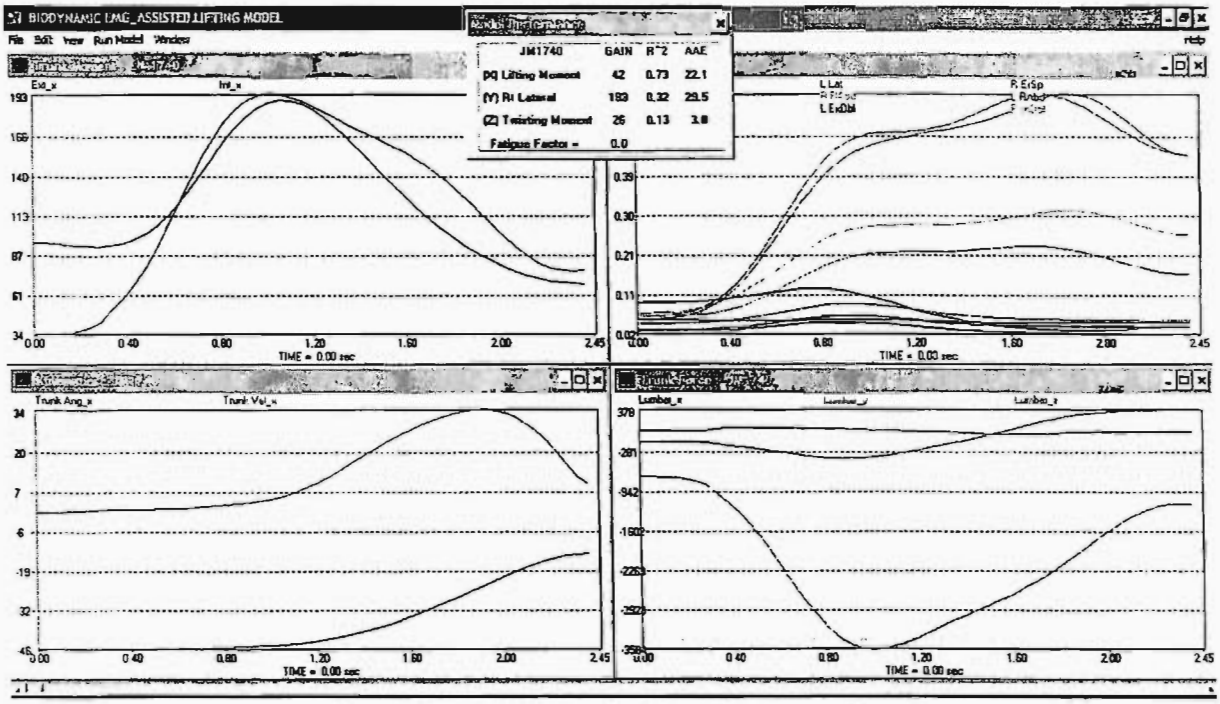

a. Actual EMG Utilized to Predict Spine Loads

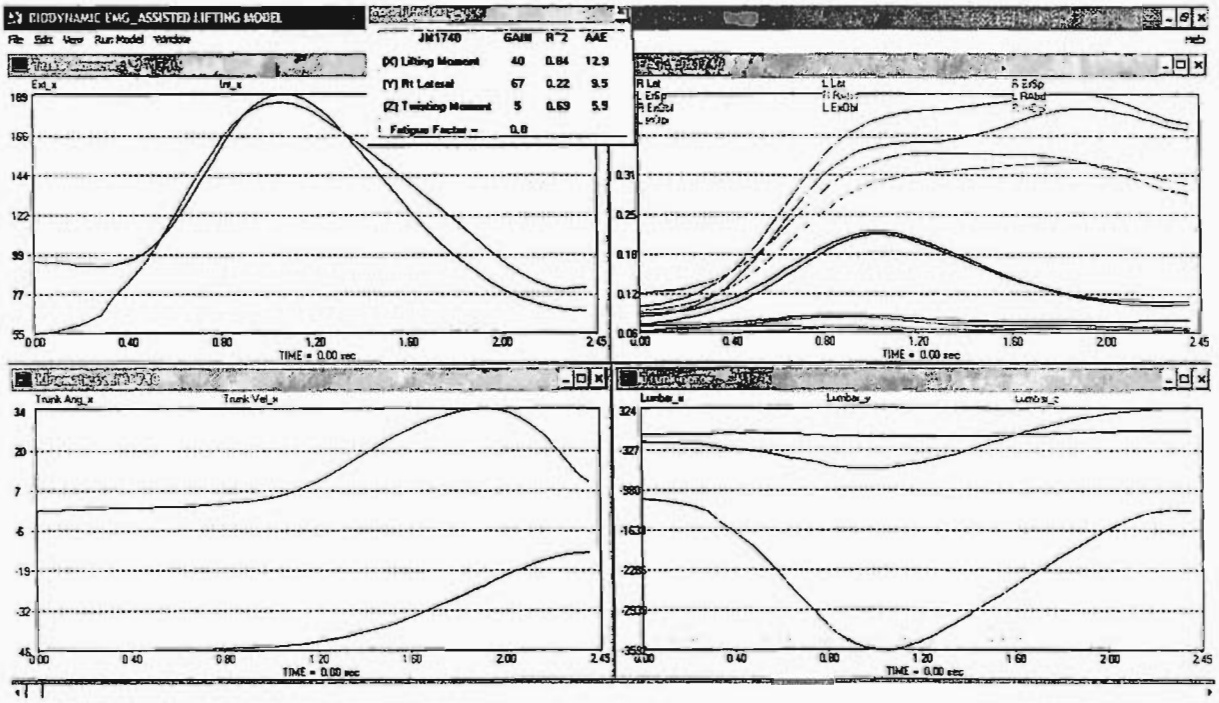

b. Predicted EMG Utilized to Predict Spine Loads

Figure 30: Second example of spine loads based on the actual and predicted EMG as predicted by the EMG-assisted model.

Articles and Presentations

Manuscripts

Lee, W., W. Karwowski, W.S. Marras, D. Rodrick, A neuro-fuzzy model for estimating electromyographical activity of trunk muscles due to manual lifting, *Ergonomics* 46 (1-3), 2003, pp. 285-309

Hou, Y., Zurada, J.M., Karwowski, W., Marras, W.S., Davis, K.G., (2007), Identification of Input Variables using Fuzzy Average with Fuzzy Cluster Distribution, *IEEE Transactions on Fuzzy Systems*, 15(4), 673-685.

Hou, Y., Zurada, J.M., Karwowski, W., Marras, W.S., Davis, K.G., (2007) Estimation of the Dynamic Spinal Forces Using a Recurrent Fuzzy Neural Network Model, *IEEE Transactions on Systems, Man, Cybernetics, Part B*, 37(1), 100-109.

Karwowski, W., Gaweda, A., Marras, W.S., Davis, K.G., Zurada, J.M., Rodrick, D., (2006), A fuzzy relational rule network modeling of electromyographical activity of trunk muscles in manual lifting based on trunk angels, moments, pelvic tilt and rotation angles. *International Journal of Industrial Ergonomics*, 36(10), 847-859.

Zurada, J., Karwowski, W. and Marras, W. S., 2004, Classification of Jobs With Risk of Low Back Disorders by Applying Data Mining Techniques, *Occupational Ergonomics,* 5 (1), 1-15, in press.

Presentation at conferences:

Karwowski, W., Gaweda, A., Marras, W.S., Davis, K.G., Zurada, J., (2003), Estimation of EMG activity of trunk muscles in manual lifting tasks based on trunk dynamics using fuzzy rational rule network. in the Proceedings of the Human Factors and Ergonomics Society 47th Annual Meeting. Denver: The Human Factors and Ergonomics Society.

Hou, Y., Zurada, J., Karwowski, W., (2004), Prediction of EMG signals of trunk muscles in manual lifting using a neural network model, in the Proceedings of 2004 IEEE International Joint Conference on Neural Networks, Budapest, Hungary.

Hou, Y., Zurada, J., Karwowski, W., (2004), Prediction of dynamic forces on lumbar joint using a recurrent neural network model, in the Proceedings of 2004 International Conference on Machine Learning and Application, Louisville, Kentucky.

Hou, Y., Zurada, J., Karwowski, W., Marras W.S., (2005), A hybrid neuro-fuzzy approach for spinal force evaluation in manual materials handling tasks, in the proceedings of 2005 International Conference on Fuzzy Systems and Knowledge Discovery, Changsha, China

Hou, Y., Zurada, J., Karwowski, W., Marras W.S., (2004), A Fuzzy Approach for Key Variables Identification of EMG Evaluation System. in the Proceedings of 2004 International Conference on Machine Learning and Application, Louisville, Kentucky.

Hou, Y., Zurada, J., Karwowski, W., Marras, W., (2006), Identification of Low Back Injury from EMG Signals using a Neural Network Model, in the Proceedings of 2006 IEEE International Joint Conference on Neural Networks, Vancouver, Canada.

Conclusions

A neural network model was built for EMG estimation. The architecture of the neural network model decomposed the lifting process in temporal domain and learned different phase of the motion separately by local connections. The global connections provided the model's basic prediction reference, while the local connections allowed the model to extract the relationships among local inputs. This modular-like organization benefited the EMG estimation performance. Subject variables were fed to the second hidden layer of the global connections. These direct feed forward connections can alleviate the curse of dimensionality and enhance the importance of subject variables. A novel fuzzy approach was employed to identify key input variables for the EMG estimation system. After training on a large data set, the developed model was able to estimate EMG using kinematic variables and subject variables. For all muscles, the overall average MAE is 7.56%; the overall average R-square is 0.5437. Thus, the model was designed to be accurately and robust with respect to predicting the muscle activity values under realistic lifting conditions. The conditions that were utilized to train the model serve as the boundary conditions. The model can then interpolate between the conditions to predict muscle activity of new conditions, reducing the necessity to collect an all encompassing data set. The structure of the model also allows the model to be continually trained when new data is acquired. A software program has been linked to a website where users can predict muscle activity from the ten trunk muscles during specific work conditions as well as upload new data to train the fuzzy engine.

Inclusion of Gender and Minority Study Populations

Since the data was collected previously, the demographic data of the subject population was already predetermined. For almost all of the studies, there was no data designating the ethnicity and race of the subjects. The only demographic data available was the age and gender of the subjects. The distribution of the database of subjects is found in the inclusion Enrollment Report below.

Inclusion of Children

While there were not specifically any children recruited and collected in the previous studies, there were 53 individuals that were between the ages of 18 and 21.

Inclusion Enrollment Report

Study Title: Derived Spine Loads in Response to Multiple Risk Factors

Total Enrollment: 239 **Protocol Number:**

Grant Number:

PART A. TOTAL ENROLLMENT REPORT: Number of Subjects Enrolled to Date (Cumulative) by Ethnicity and Race

Ethnic Category	Sex/Gender			
	Females	Males	Unknown or Not Reported	Total
Hispanic or Latino				**
Not Hispanic or Latino				
Unknown (individuals not reporting ethnicity)	85	154		239
Ethnic Category: Total of All Subjects*	85	154		239 *
Racial Categories				
American Indian/Alaska Native				
Asian				
Native Hawaiian or Other Pacific Islander				
Black or African American				
White				
More Than One Race				
Unknown or Not Reported	85	154		239
Racial Categories: Total of All Subjects*	85	154		239 *

PART B. HISPANIC ENROLLMENT REPORT: Number of Hispanics or Latinos Enrolled to Date (Cumulative)

Racial Categories	Females	Males	Unknown or Not Reported	Total
American Indian or Alaska Native				
Asian				
Native Hawaiian or Other Pacific Islander				
Black or African American				
White				
More Than One Race				
Unknown or Not Reported			239	239
Racial Categories: Total of Hispanics or Latinos**			239	239 **

References:

[1] Praemer, A., S. Furner, and D.P. Rice, Musculoskeletal Conditions in the United States. 1992, American Academy of Orthopaedic Surgeons: Park Ridge, IL. p. Pg.23-33.

[2] Hollbrook, T.L., et al., The Frequency of Occurrence, Impact and Cost of Selected Musculoskeletal Conditions in the United States. 1984, Chicago, IL: American Academy of Orthopaedic Surgeons. pg. 24-45.

[3] Guo, H.R. Back Pain and U.S. Workers. in American Occupational Health Conference. 1993: (NIOSH Report).

[4] Andersson, G.B., The epidemiology of spinal disorders, in The Adult Spine: Principles and Practice, J.W. Frymoyer, Editor. 1997, Lippincott-Raven Publishers: Philadelphia. p. 93-141.

[5] Pope, M.H. Muybridge Lecture. in International Society of Biomechanics XIVth Congress. 1993. Paris, France.

[6] Frymoyer, J.W., et al., Risk Factors in Low Back Pain: An Epidemiologic Survey. *J. Bone Joint Surg.*, 1983. 65A: p. 213-216.

[7] Webster, B.S. and S.H. Snook, The Cost of Compensable Low Back Pain. 1989, Liberty Mutual internal report.

[8] Cats-Baril, W. and J.W. Frymoyer, The Economics of Spinal Disorders, in The Adult Spine, J.W. Frymoyer, et al., Editors. 1991, Raven Press: New York, NY. p. 85-105.

[9] National Safety Council, Accident Facts, 1989. 1989: Chicago, IL.

[10] Andersson, G.B., Epidemiologic aspects on low-back pain in industry. *Spine*, 1981. 6(1): p. 53-60.

[11] Bernard, B.P., Musculoskeletal disorders and workplace factors: A critical review of epidemiologic evidence for work-related musculoskeletal disorders of the neck, upper extremity, and low back. Vol. publication No. 97-141, National Institute for Occupational Safety and Health. 1997, Cincinnati, Ohio: U.S. Department of Health and Human Services (DHHS).

[12] Burdorf, A. and G. Sorock, Positive and negative evidence of risk factors for back disorders. *Scand J Work Environ Health*, 1997. 23(4): p. 243-56.

[13] Bigos, S.J., et al., Back injuries in industry: a retrospective study. II. Injury factors. *Spine*, 1986. 11(3): p. 246-51.

[14] Snook, S.H., The Control of Low Back Disability: The Role of Management in Manual Materials Handling: Understanding and Preventing Back Trauma. 1989, American Industrial Hygiene Association: Akron, OH.

[15] Spengler, D.M., et al., Back injuries in industry: a retrospective study. I. Overview and cost analysis. *Spine*, 1986. 11(3): p. 241-5.

[16] Marras, W.S., et al., Prospective validation of a low-back disorder risk model and assessment of ergonomic interventions associated with manual materials handling task. *Ergonomics*, 2000. 43(11): p. 1866-86.

[17] Marras, W.S., et al., The role of dynamic three-dimensional trunk motion in occupationally- related low back disorders. The effects of workplace factors, trunk position, and trunk motion characteristics on risk of injury. *Spine*, 1993. 18(5): p. 617-28.

[18] Marras, W.S., et al., Biomechanical risk factors for occupationally related low back disorders. *Ergonomics*, 1995. 38(2): p. 377-410.

[19] Norman, R., et al., A comparison of peak vs cumulative physical work exposure risk factors for the reporting of low back pain in the automotive industry. *Clinical Biomechanics*, 1998. 13: p. 561-573.

[20] Granata, K.P. and W.S. Marras, An EMG-assisted model of loads on the lumbar spine during asymmetric trunk extensions. *J Biomech*, 1993. 26(12): p. 1429-38.

[21] Granata, K.P. and W.S. Marras, An EMG-assisted model of trunk loading during free-dynamic lifting. *J Biomech*, 1995. 28(11): p. 1309-17.

[22] Granata, K.P. and W.S. Marras, Relation between spinal load factors and the high-risk probability of occupational low-back disorder. *Ergonomics*, 1999. 42(9): p. 1187-99.

[23] Marras, W.S. and K.P. Granata, A biomechanical assessment and model of axial twisting in the thoracolumbar spine. *Spine*, 1995. 20(13): p. 1440-51.

[24] Marras, W.S. and K.P. Granata, Spine loading during trunk lateral bending motions. *J Biomech*, 1997. 30(7): p. 697-703.

[25] Marras, W.S. and K.P. Granata, Changes in trunk dynamics and spine loading during repeated trunk exertions. *Spine*, 1997. 22(21): p. 2564-70.

[26] Marras, W.S., et al., The effectiveness of commonly used lifting assessment methods to identify industrial jobs associated with elevated risk of low-back disorders. *Ergonomics*, 1999. 42(1): p. 229-45.

[27] Marras, W.S. and K.G. Davis, Spine loading during asymmetric lifting using one versus two hands. *Ergonomics*, 1998. 41(6): p. 817-34.

[28] Marras, W.S., et al., Effects of box features on spine loading during warehouse order selecting. *Ergonomics*, 1999. 42(7): p. 980-96.

[29] Davis, K.G., W.S. Marras, and T.R. Waters, The evaluation of spinal loads during lowering and lifting. *Clin Biomech*, 1998. 13(3): p. 141-52.

[30] Davis, K.G., W.S. Marras, and T.R. Waters, Reduction of spinal loading through the use of handles. *Ergonomics*, 1998. 41(8): p. 1155-68.

[31] Davis, K.G. and W.S. Marras, Assessment of the relationship between box weight and trunk kinematics: does a reduction in box weight necessarily correspond to a decrease in spinal loading? *Human Factors*, 2000. 42(2): p. 195-208.

[32] Marras, W.S., et al., Spine loading and trunk kinematics during team lifting. *Ergonomics*, 1999. 42(10): p. 1258-73.

[33] Marras, W.S., et al., A comprehensive analysis of low-back disorder risk and spinal loading during the transferring and repositioning of patients using different techniques. *Ergonomics*, 1999. 42(7): p. 904-26.

[34] Marras, W.S., S.L. Rangarajulu, and P.E. Wongsam, Trunk force development during static and dynamic lifts. *Human Factors*, 1987. 29(1): p. 19-29.

[35] Marras, W.S. and G.A. Mirka, Muscle activities during asymmetric trunk angular accelerations. *J Orthop Res*, 1990. 8(6): p. 824-32.

[36] Marras, W.S. and G.A. Mirka, A comprehensive evaluation of trunk response to asymmetric trunk motion. *Spine*, 1992. 17(3): p. 318-26.

[37] Bongers, P.M., et al., Psychosocial factors at work and musculoskeletal disease. *Scand J Work Environ Health*, 1993. 19(5): p. 297-312.

[38] Burton, A.K., et al., Psychosocial predictors of outcome in acute and subchronic low back trouble. *Spine*, 1995. 20(6): p. 722-8.

[39] Krause, N., et al., Psychosocial job factors, physical workload, and incidence of work-related spinal injury: a 5-year prospective study of urban transit operators. *Spine*, 1998. 23(23): p. 2507-16.

[40] Davis, K.G and C.A. Heaney, The relationship between psychosocial work characteristics and low back pain: underlying methodological issues. *Clin Biomech* (Bristol, Avon), 2000. 15(6): p. 389-406.

[41] Hoogendoorn, W.E., et al., Systematic review of psychosocial factors at work and private life as risk factors for back pain. *Spine*, 2000. 25(16): p. 2114-25.

[42] Marras, W.S., et al., The Influence of Psychosocial Stress, Gender, and Personality on Mechanical Loading of the Lumbar Spine. *Spine*, 2000. 25(23): p. 3045-3054.

[43] Thorbjornsson, C.B., et al., Physical and psychosocial factors related to low back pain during a 24- year period. A nested case-control analysis. *Spine*, 2000. 25(3): p. 369-74; discussion 375.

[44] Hoogendoorn, W.E., et al., Psychosocial work characteristics and psychological strain in relation to low-back pain. *Scand J Work Environ Health*, 2001. 27(4): p. 258-67.

[45] Karjalainen, K., et al., Multidisciplinary Biopsychosocial Rehabilitation for Subacute Low Back Pain in Working-Age Adults: A Systematic Review Within the Framework of the Cochrane Collaboration Back Review Group. *Spine*, 2001. 26(3): p. 262-269.

[46] Kerr, M.S., et al., Biomechanical and psychosocial risk factors for low back pain at work. *Am J Public Health*, 2001. 91(7): p. 1069-75.

[47] MacDonald, L.A., et al., Covariation between workplace physical and psychosocial stressors: evidence and implications for occupational health research and prevention. *Ergonomics*, 2001. 44(7): p. 696-718.

[48] Davis, K.G, et al., Influence of lift moment in determining MAWL. *Human Factors*, 1997. 39(2): p. 312-22.

[49] Davis, K.G, M.J. Jorgensen, and W.S. Marras, An investigation of perceived exertion via whole body exertion and direct muscle force indicators during the determination of the maximum acceptable weight of lift. *Ergonomics*, 2000. 43(2): p. 143-59.

[50] Jorgensen, M.J., et al., Significance of biomechanical and physiological variables during the determination of maximum acceptable weight of lift. *Ergonomics*, 1999. 42(9): p. 1216-32.

[51] Davis, K.G, W.S., Marras, C.A., Heaney, T.R., Waters, P., Gupta, (2002), The impact of mental processing and pacing on spine loading, *Spine*, 27(23), 2645-2653.

[52] Chaffin, D.B. and K.S. Park, A longitudinal study of low-back pain as associated with occupational weight lifting factors. *Am Ind Hyg Assoc J*, 1973. 34(12): p. 513-25.

[53] Cherniack, M., et al., Clincial and psychological correlates of lumbar motion abnormalities in low back pain. *The Spine Journal*, 2001. 1(4): p. 290-298.

[54] Marras, W.S., et al., The classification of anatomic- and symptom-based low back disorders using motion measure models. *Spine*, 1995. 20(23): p. 2531-46.
[55] Marras, W.S., et al., The quantification of low back disorder using motion measures. Methodology and validation. *Spine*, 1999. 24(20): p. 2091-100.
[56] Deyo, R.A. and J.E. Bass, Lifestyle and low-back pain. The influence of smoking and obesity. *Spine*, 1989. 14(5): p. 501-6.
[57] Kelsey, J.L. and A.M. Ostfeld, Demographic characteristics of persons with acute herniated lumbar intervertebral disc. *J Chronic Dis*, 1975. 28(1): p. 37-50.
[58] Kelsey, J.L., et al., Acute prolapsed lumbar intervertebral disc. An epidemiologic study with special reference to driving automobiles and cigarette smoking. *Spine*, 1984. 9(6): p. 608-13.
[59] Allread, W.G., W.S., Marras, Does personality affect the risk of developing musculoskeletal discomfort? *Theoretical Issues in Ergonomic Science*, 7(2), p.149-167.
[60] Marras, W.S., et al., Spine loading characteristics of patients with low back pain compared with asymptomatic individuals. *Spine*, 2001. 26(23): p. 2566-74.
[61] Nachemson, A., Towards a better understanding of low-back pain: a review of the mechanics of the lumbar disc. *Rheumatol Rehabil*, 1975. 14(3): p. 129-43.
[62] Videman, T., M. Nurminen, and J.D. Troup, 1990 Volvo Award in clinical sciences. Lumbar spinal pathology in cadaveric material in relation to history of back pain, occupation, and physical loading. *Spine*, 1990. 15(8): p. 728-40.
[63] National Research Council, Musculoskeletal disorders and the workplace: low back and upper extremity. 2001, Washington D.C.: National Academy Press.
[64] Buckwalter, J.A., Aging and degeneration of the human intervertebral disc. *Spine*, 1995. 20(11): p. 1307-14.
[65] Jager, M., A. Luttmann, and W. Laurig, Lumbar load during one-hand bricklaying. *Int J Indust Ergo*, 1991. 8: p. 261-277.
[66] Kauppila, L.I., Prevalence of stenotic changes in arteries supplying the lumbar spine. A postmortem angiographic study on 140 subjects. *Ann Rheum Dis*, 1997. 56(10): p. 591-5.
[67] Porter, R.W., M.A. Adams, and W.C. Hutton, Physical activity and the strength of the lumbar spine. *Spine*, 1989. 14(2): p. 201-3.
[68] Marras, W.S., K.G. Davis, and K.P. Granata, Trunk muscle activities during asymmetric twisting motions. *J Electromyogr Kinesiol*, 1998. 8(4): p. 247-56.
[69] Schultz, A., et al., Lumbar trunk muscle use in standing isometric heavy exertions. *J Orthop Res*, 1987. 5(3): p. 320-9.
[70] Adams, M.A., et al., Mechanical Initiation of Intervertebral Disc Degeneration. *Spine*, 2000. 25(13): p. 1625-1636.
[71] Adams, M.A., et al., Sustained loading generates stress concentrations in lumbar intervertebral discs. *Spine*, 1996. 21(4): p. 434-8.
[72] Adams, M.A. and W.C. Hutton, Gradual disc prolapse. *Spine*, 1985. 10(6): p. 524-31.
[73] Brinkmann, P., M. Biggermann, and D. Hilweg, Fatigue fracture of human lumbar vertebrae. *Clin Biomech*, 1988. 3(Suppl. 1): p. S1-S23.

[74] Callaghan, J.P. and S.M. McGill, Intervertebral disc herniation: studies on a porcine model exposed to highly repetitive flexion/extension motion with compressive force. *Clin Biomech*, 2001. 16(1): p. 28-37.

[75] Yingling, V.R. and S.M. McGill, Anterior shear of spinal motion segments. Kinematics, kinetics, and resultant injuries observed in a porcine model. *Spine*, 1999. 24(18): p. 1882-9.

[76] Cavanaugh, J.M., et al., Mechanisms of low back pain: a neurophysiologic and neuroanatomic study. *Clin Orthop*, 1997(335): p. 166-80.

[77] Bogduk, N., The anatomical basis for spinal pain syndromes. *J Manipulative Physiol Ther*, 1995. 18(9): p. 603-5.

[78] Siddall, P.J. and M.J. Cousins, Spinal pain mechanisms. *Spine*, 1997. 22(1): p. 98-104.

[79] Bartlett, E.B. Self Determination of Input Variable Importance by Neural Networks, Neural, Parallel and Scientific Computations, 2(1), 1994 pp. 103-114.

[80] Yuan, B., G. Klir, Intelligent Hybrid Systems-Fuzzy Logic, Neural Networks, and Genetic Algorithms, Da Ran, Kluwer Academic Publishers, 1999 pp. 161-186.

[81] Sugeno, M., T. Yasukawa, A fuzzy-logic-based approach to qualitative modeling, *IEEE Trans. on Fuzzy Systems*, 1 (1), 1993. pp. 7-31.

[82] Chiu, S. L., Selecting input variables for fuzzy models, *Journal of Intelligent and Fuzzy Systems*, 4, 1996, pp. 243-256.

[83] Lin, Y., G.A. Cunningham, A new approach to fuzzy-neural system modeling"; *IEEE Trans. on Fuzzy Systems*, 3(2), 1995, pp. 190-198.

[84] Lin, Y., G.A. Cunningham, S.V. Coggeshall, R.D. Jones, Nonlinear system input structure identification: two stage fuzzy curves and surfaces; *IEEE Trans. on Systems, Man and Cybernetics, Part A*, 28(5), 1998 pp. 678 -684.

[85] Azeem, M.F., M. Hanmandlu, N. Ahmad, Structure identification of generalized adaptive neuro-fuzzy inference systems, *IEEE Trans. on Fuzzy Systems*,11(5), 2003, pp. 666-681.

[86] Morabito, E.C., M. Versaci, A fuzzy neural approach to localizing holes in conducting plates; *IEEE Trans. on Magnetics*, 37(5), 2001 pp. 3534-3537.

[87] Papadakis, S.E., J.B. Theocharis, J. Kiartzis, A.G. Bakirtzis, A novel approach to short-term load forecasting using fuzzy neural networks; *IEEE Trans. on Power Systems*, 13(2), 1998, pp. 480-492.

[88] Sung, A.H., Ranking input importance in neural network modeling of engineering problems, *Proc. of IEEE World Congress on Computational Intelligence*, 1, 1998, pp. 316-321.

[89] Bouqata, B., A. Bensaid, R. Palliam, A.F.G. Skarmeta, Time series prediction using crisp and fuzzy neural networks: a comparative study, P*roc. of the IEEE/IAFE/INFORMS 2000 Conf. on Computational Intelligence for Financial Engineering*, 2000, pp. 170-173.

[90] Azeem, M.F., M. Hanmandlu, N. Ahmad, A new criteria for input variable identification of dynamical systems; *Proc. of IEEE Region 10 Int. Conf. on Global Connectivity in Energy, Computer, Communication and Control*, 1, 1998, pp. 230-233.

[91] Morabito, F.C., M. Versaci, A fuzzy-neural approach to real time plasma boundary reconstruction in tokamak reactors, *Proc. of Int. Conf. on Neural Networks*, 1, 1997, pp. 43 -47.

[92] Papadakis, S., J. Theocharis, An efficient fuzzy neural modeling approach using the fuzzy curve concept; *Proc. of the Third IEEE Int. Conf. on Electronics, Circuits, and Systems*, 1, 1996, pp. 279-282.

[93] Schrich, E.S., J. Ke, L.O. Hall, D.B. Goldgof, Fast accurate fuzzy clustering through data reduction; *IEEE Transaction on Fuzzy Systems*, 11 (2), 2003.

[94] Auephanwiriyakul, S., J. M. Keller, Analysis and efficient implementation of a linguistic fuzzy c-means, *IEEE Trans. on Fuzzy Systems*, 10(5), 2002, pp. 563-582.

[95] Wang, L., T.S. Buchanan, Prediction of Joint Moments Using a Neural Network Model of Muscle Activations from EMG Signals, *IEEE Transactions on Systems and Rehabilitation Engineering*, 10(1), 2002, p. 30-37.

[96] Arthur, T.C., F.K. Robert, EMG-based Prediction of Shoulder and Elbow Kinematics in Able-bodied and Spinal Cord Injured Individuals, *IEEE Transactions on Rehabilitation Engineering*, 8(4), 2000 p. 471-480.

[97] Pattichis, C.S., C.N. Schizas, Genetics-based Machine Learning for the Assessment of Certain Neuromuscular Disorders, *IEEE Transactions on Neural Networks*, 7(2), 1996, p. 427-439.

[98] Lee, W., W. Karwowski, W.S. Marras, D. Rodrick, A neuro-fuzzy model for estimating electromyographical activity of trunk muscles due to manual lifting, *Ergonomics* 46(1-3), 2003, p. 285-309.

[99] Chen, S.T., D.C. Yu, and Moghaddamjo, A.R., (1992), Weather Sensitive Short-Term Load Forecasting Using Nonfully Connected Artificial Neural Network, *IEEE Transactions on Power Systems*, 7(3), p. 1098-1105.

[100] Wang, l., S.Z. Der, N.M. Nasrabadi, Automatic target recognition using a feature-decomposition and data-decomposition modular neural network, *IEEE Transactions on Image Processing*, 7(8), 1998, p. 1113-1121

[101] Hong, T., M.T.C. Fang, Detection and classification of partial discharge using a feature decomposition-based modular neural network, *IEEE Transactions on Instrumentation and Measurement*, 50(5), 2001, p. 1349-1354.

[102] Anand, R., K. Mehrotra, C.K. Mohan, S. Ranka, Efficient classification for multiclass problems using modular neural networks, *IEEE Transactions on Neural Networks*, 6(1), 1995, p. 117-124.

[103] Khotanzad, A., R.C. Hwang, A. Abaye, D. Maratukulam, An adaptive modular artificial Neural network hourly load forecaster and its implementation at electric utilities, *IEEE Transactions on Power Systems*, 10(3), 1995, p. 1716-1722.

[104] Lu, B.L., J. Shin, M. Ichikawa, Massively parallel classification of single-trial EEG signals using a min-max Modular neural network, *IEEE Transactions on Biomedical Engineering*, 51(3), 2004, p. 551-558.

[105] Jacobs, R.A., M. I. Jordan, Learning piecewise control strategies in a modular neural network architecture, *IEEE Transactions on Systems, Man and Cybernetics*, 23(2), 1993, p. 337-345.

[106] Haykin, S., Neural Networks, A Comprehensive Foundation. New York: MacMillian, 1994.

[107] Poulton, M.M., R. A. Birken, Estimating one-dimensional models from frequency-domain electromagnetic data using modular neural networks, *IEEE Transactions on Geoscience and Remote Sensing*, 36(2), 1998, p. 547-555.

[108] Jacobs, R.A., M. I. Jordan, S. J. Nowlan, and G. E. Hinton, Adaptive mixtures of local experts", *Neural Comput.*, 3, 1991, pp. 79-877.

[109] Perrone, M.P., General averaging results for convex optimization, in *Proc. Connectionist Models Summer School*, 1993, p. 364-371.